




## Review

# 3D Solar Harvesting and Energy Generation via Multilayers of Transparent Porphyrin and Iron Oxide Thin Films

Jou Lin , Mengyao Lyu  and Donglu Shi \* 

The Materials Science and Engineering Program, Department of Mechanical and Materials Engineering, College of Engineering and Applied Science, University of Cincinnati, Cincinnati, OH 45221, USA

\* Correspondence: shid@ucmail.uc.edu

**Abstract:** Photovoltaic solar cells have been extensively used for various applications and are considered one of the most efficient green energy sources. However, their 2D surface area solar harvesting has limitations, and there is an increasing need to explore the possibility of multiple layer solar harvest for enhanced energy density. To address this, we have developed spectral-selective transparent thin films based on porphyrin and iron oxide compounds that allow solar light to penetrate multiple layers, significantly increasing solar harvesting surface area and energy density. These thin films are designed as photovoltaic (PV) and photothermal (PT) panels that can convert photons into either electricity or thermal energy for various green energy applications, such as smart building skins and solar desalination. The advantages of this 3D solar harvesting system include enlarged solar light collecting surface area and increased energy density. The multilayer system transforms the current 2D to 3D solar harvesting, enabling efficient energy generation. This review discusses recent developments in the synthesis and characterization of PV and PT transparent thin films for solar harvesting and energy generation using multilayers. Major applications of the 3D solar harvesting system are reviewed, including thermal energy generation, multilayered DSSC PV system, and solar desalination. Some preliminary data on transparent multilayer DSSC PVs are presented.

**Keywords:** spectral-selective solar harvesting; multilayer system; photothermal energy generation; 3D desalination



**Citation:** Lin, J.; Lyu, M.; Shi, D. 3D Solar Harvesting and Energy Generation via Multilayers of Transparent Porphyrin and Iron Oxide Thin Films. *Energies* **2023**, *16*, 3173. <https://doi.org/10.3390/en16073173>

Academic Editor: Antonio Calvo Hernández

Received: 26 February 2023

Revised: 14 March 2023

Accepted: 25 March 2023

Published: 31 March 2023



**Copyright:** © 2023 by the authors. Licensee MDPI, Basel, Switzerland. This article is an open access article distributed under the terms and conditions of the Creative Commons Attribution (CC BY) license (<https://creativecommons.org/licenses/by/4.0/>).

## 1. Introduction

To produce clean energy and develop sustainable green/blue infrastructures, solar energy utilization has been a popular approach due to its technical, environmental, and ecological advantages [1–5]. Photovoltaic (PV) solar cells have been widely used for various applications, including solar energy utilities [6–9]. However, the 2D surface solar harvesting of PV cells has limitations. To meet the total yearly electricity demand of the United States, an estimated 13,600,000 acres of solar panels would be required assuming 4 petawatt hours of electricity per year [10]. However, not all lands are available for solar cells, particularly in densely populated megacities where limited roof space can reduce the potential for solar harvesting. In such cases, alternative solutions, such as community solar gardens or building-integrated photovoltaics (BIPV), may be needed to meet the energy needs of the city [11–18].

There is a growing need for more efficient solar harvesting approaches that can significantly increase photon collection area within a confined volume. Multilayer photovoltaic (PV) and photothermal (PT) solar harvesting offer a way to increase the energy density of a solar system by stacking multiple layers of PV or PT films on top of each other. This results in more compact and efficient use of space compared to traditional single-layer solar panels. Transparent thin films allow solar light to pass through multiple layers for either PV or PT photon conversion and energy generation. By stacking multiple layers, the PV and PT films can increase the amount of electricity or thermal energy generated per unit of volume.

Both photothermal (PT) [18–29] and photovoltaic (PV) thin films [1–5,30–34] have been used for solar harvesting and energy generation. The former converts photons to thermal energy while the latter generates electricity through different mechanisms, with both characterized by power conversion efficiency (PCE). To achieve solar harvesting in a three-dimensional (3D) fashion, spectral-selective transparent thin films have been developed, analogous to multilayer capacitors that increase the total surface area within a finite volume. As shown in Figure 1, sunlight can pass through multiple layers of transparent substrates and generate energy through either PT or PV. For multilayer solar harvesting, both PT and PV thin films need to be transparent with high average visible transmittance (AVT). Furthermore, specific optical characteristics of PT or PV are required for optimal energy conversion. For a highly transparent PT film, absorptions should be concentrated in the UV and IR regions for photon conversion to thermal heat, while those in the visible band should be kept at a minimum for high AVT.

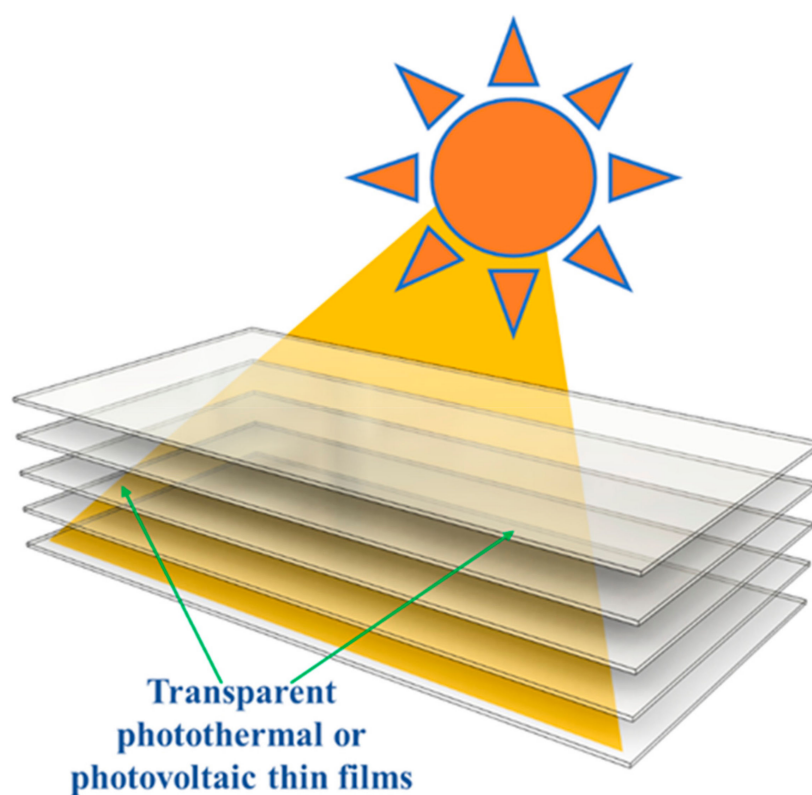


**Figure 1.** Schematic diagram showing the concept of 3D multilayer solar light harvesting.

However, the optical absorption requirements for photovoltaics (PV) are distinctively different. It is well known that the power conversion efficiency (PCE) of PV cannot surpass the Shockley–Queisser limit (SQ limit) [34]. The SQ model is established based on intrinsic limitations, such as blackbody radiation, recombination, and spectral losses. The spectral losses are limited by the bandgap energy ( $E_g$ ). Photons with energies lower than  $E_g$  do not contribute to the short-circuit current ( $I_{sc}$ ) of the solar panel [35]. For instance, in the case of silicon, with an  $E_g$  of 1.1 eV, about 19% of photons have energies lower than 1.1 eV, which constitutes around 33% of the incident sunlight. The spectral response is the ratio of current generated by the solar panel to the power incident on it. The high-energy photons close to the ultraviolet (UV) spectrum contribute to thermalization for silicon semiconductors [36]. Based on these considerations, the SQ limit predicts a maximum PCE of 33.7% for a single p-n junction with a bandgap of 1.4 eV [34].

We have developed transparent PT and PV films for solar harvest and energy generation [19–30]. These materials have varying optical characteristics and are used in different applications, such as solar desalination, photothermal energy generation, and smart build-

ing skins [20–22,26–29]. Figure 2 displays the absorption spectra of various materials, with gold nanoparticles [37] exhibiting strong absorption below 300 nm and a peak at 520 nm for visible light absorption. Graphene [38] and  $\text{Fe}_3\text{O}_4$  nanoparticles [24–27] have stronger absorption in the UV range, gradually declining to the visible range and near infrared. The porphyrin compound chlorophyll [20,21], including its derivatives, such as chlorophyllin [21], displays a saddle-shaped spectrum with two peaks near 400 nm (blue–violet) and 700 nm (NIR). The  $\text{Fe}_3\text{O}_4@\text{Cu}_{2-x}\text{S}$  thin films have a broad NIR absorption due to their core–shell structure, characterized by a “U”-shaped spectrum that is ideal for multilayer solar harvesting [26–29]. The desired spectrum for PT, shown by a dashed line, has maximum UV and NIR absorption and high transmittance in the visible range.

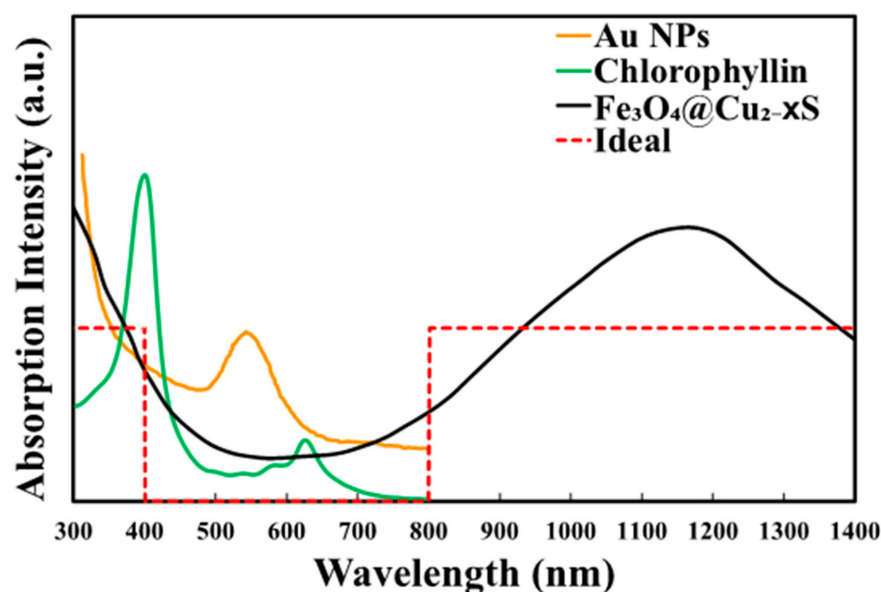


Figure 2. Optical absorption spectra of different materials as indicated.

By considering the unique optical characteristics of various materials, such as porphyrins and iron oxides, a 3D solar harvesting system (Figure 1) can be constructed to directly convert light into different forms of energy for a wide range of applications. Transparent multilayers of spectral-selective thin films allow solar light to pass through, generating electricity via PV or thermal energy through PT at each layer collectively to produce efficient energy generation and conversion. This approach is fundamentally distinct from the current 2D PV panels, which have limited surface areas for solar harvesting. The multilayer concept revolutionizes the current 2D PV and transforms solar harvesting to 3D using transparent thin films, significantly increasing the sunlight collecting area and energy density in a limited space. Various energy harvesting systems based on different porphyrin and iron oxide compounds are introduced in this paper.

Two types of materials, iron oxides and porphyrins, were synthesized for PT and PV applications in previous works [19–30]. Iron oxides have been widely researched on small quantities of nanoparticles in solutions for medical theranostics [39–42], but few studies have been conducted on their use in transparent, robust thin films for energy applications [18–29]. In our laboratory, we have recently developed  $\text{Fe}_3\text{O}_4@\text{Cu}_{2-x}\text{S}$  transparent thin films that exhibit enhanced IR absorptions compared to  $\text{Fe}_3\text{O}_4$  [26]. This material system displays strong UV and NIR absorptions that can be photonicly activated to test its 3D solar harvesting capabilities via the photothermal effect. Using thermal energy converted from the photons on the multilayers, we were able to determine the solar harvesting and energy conversion efficiencies of the 3D solar harvesting system.

Porphyrin compounds are well-known for their optical and photosynthetic characteristics [43–46]. Some bio-inspired materials, such as chlorophyll, have been found to exhibit PV effects and are used as transparent organic photovoltaics (TOPV) [47–50]. Porphyrins are organic compounds that occur widely in nature and consist of a central metal ion, usually iron or magnesium, surrounded by a ring of nitrogen atoms [43–46]. The ring is made up of four pyrrole molecules that are connected by methine bridges. Porphyrins play a crucial role in various biological processes, including energy metabolism and oxygen transport. They have a wide range of applications in fields such as biochemistry, medicine, and chemistry. For example, porphyrins are used as catalysts in chemical reactions [43] and as photosensitizers in photothermal/photodynamic therapy [39]. Furthermore, porphyrins possess unique optical and electronic properties that make them suitable for developing advanced materials and technologies, such as photovoltaic cells and molecular electronics [47–50]. However, their potential for 3D solar harvesting on transparent thin films or for photothermal energy generation has not been explored. In this study, we investigated chlorophyllin thin films for their PT and PV effects in 3D solar harvesting and energy generation.

## 2. Synthesis and Characterization of the Porphyrin Compounds

A family of organic compounds with a heterocyclic macrocycle structure known as porphyrins share a common feature of a ring-like structure composed of four modified subunits bonded with carbon atoms (Figure 3) [51]. This structure contains 26  $\pi$ -electrons, with 18 of them forming a continuous cycle of conjugated bonds as shown in Figure 3. Examples of porphyrin compounds include chlorophyll (Chl), chlorophyllin (Chlin), hemoglobin (HB), and phthalocyanine (Phth) [21].

These compounds are well-known for their distinctive and intrinsic photon absorption spectra over a wide range of frequencies, which are specifically linked to the metal ion that is bonded to all four nitrogens [46]. For instance, chlorophyll, which has a magnesium center atom (Figure 3a), exhibits a saddle-shaped absorption spectrum with main absorptions in the UV and NIR regions (Figure 3a), resulting in its green color. By substituting the center metal atom with copper, chlorophyllin is formed, which displays two absorption peaks at 415 and 664 nm (Figure 3b). Hemoglobin and phthalocyanine both have strong UV absorptions. Notably, hemoglobin lacks NIR absorption (Figure 3c), whereas phthalocyanine has a broad absorption band in the NIR region (Figure 3d) [21].

Other porphyrin compounds were synthesized according to the procedures outlined in References [20,21]. Chlorophyll was extracted from spinach following a previously reported method (Refs. [20,21]). Briefly, fresh local spinach leaves were cut into small pieces ( $\sim 5 \times 5$  mm<sup>2</sup>) and then freeze-dried at  $-40$  °C for 48 h. The resulting dry leaves (5 g) were washed twice with petroleum ether (boiling point 40–60 °C) to remove the carotenoids and waxes. The washed leaves were then immersed and stirred in 300 mL of methanol/petroleum ether (3:1 *v/v*) at room temperature overnight. Any remaining solids were removed by filtration, and the resulting solutions were transferred to a separatory funnel and washed twice with 200 mL of saturated sodium chloride solution. The organic phase was filtrated and removed by rotary evaporation. The isolated film was then dissolved in 50 mL of acetone and stored at  $-20$  °C for 24 h to precipitate impurities. The precipitates were pelleted by centrifugation, and the supernatant was collected. The isolated chlorophyll was dissolved in toluene and stored at  $-20$  °C until use. Chlorophyllin sodium copper was purchased from Sigma-Aldrich (St. Louis, MO, USA). For thin film deposition, the chlorophyllin solution was mixed with PEG in water.



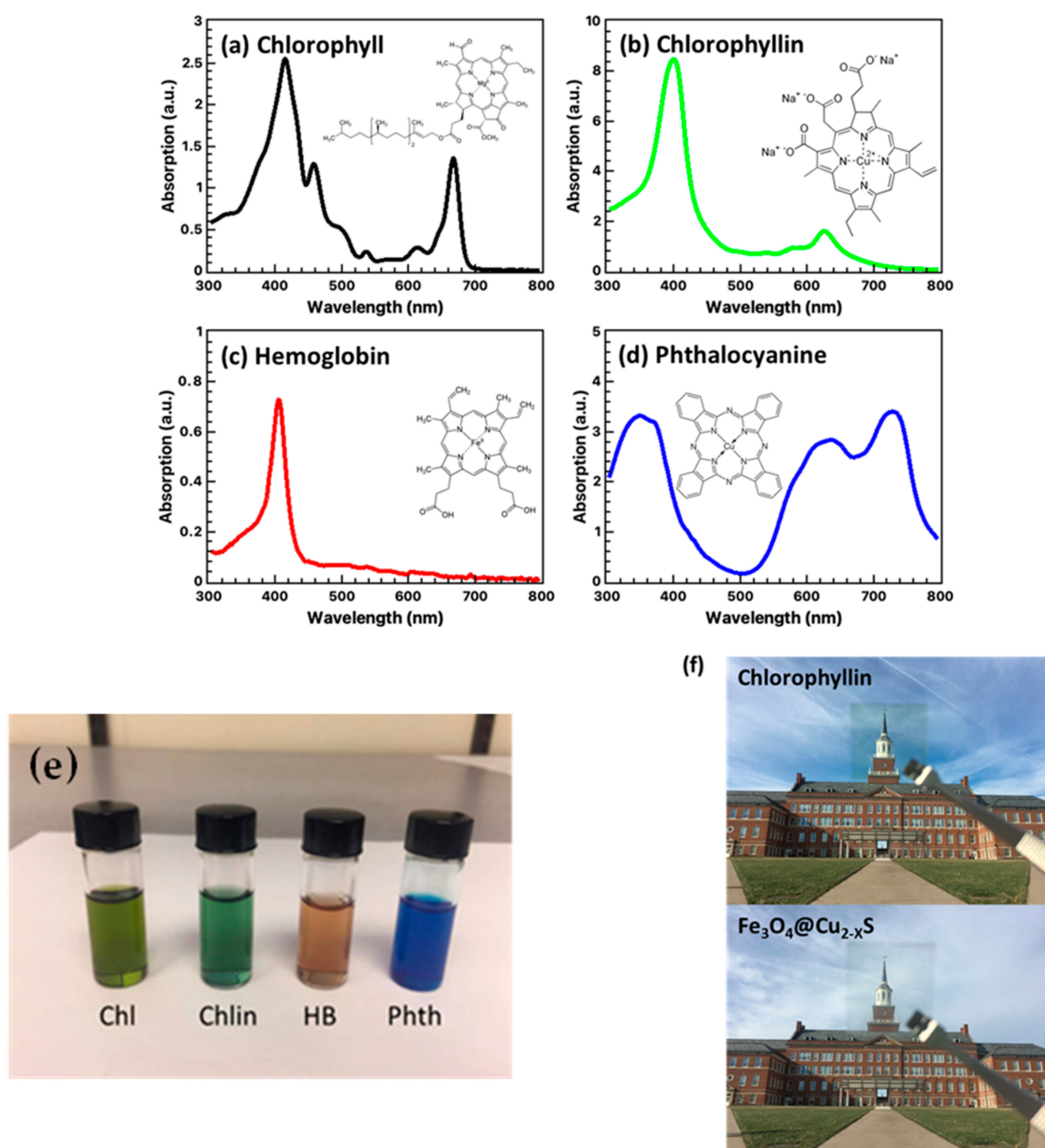


**Figure 3.** (a) Chlorophyll structure and absorption, (b) chlorophyllin structure and absorption, (c) hemoglobin and absorption, (d) phthalocyanine and absorption, (e) solutions of these porphyrin compounds, and (f) photographs of transparent chlorophyllin and  $\text{Fe}_3\text{O}_4@\text{Cu}_{2-x}\text{S}$  [21].

### 3. Synthesis and Characterization of the Iron Oxide Nanoparticles

$\text{Fe}_3\text{O}_4$  nanoparticles have been extensively researched for various applications in biomedicine, environmental protection, and materials science due to their magnetic, electronic, and optical properties [23–25]. They have been used as contrast agents for magnetic resonance imaging (MRI), in photothermal therapy, targeted drug delivery, magnetic data storage, and as catalysts for chemical reactions [52–55]. The  $\text{Fe}_3\text{O}_4@\text{Cu}_{2-x}\text{S}$  composite material, which consists of  $\text{Fe}_3\text{O}_4$  nanoparticles coated with a shell of copper sulfide ( $\text{Cu}_{2-x}\text{S}$ ) [27], has potential applications in various fields due to its unique IR absorptions [56–60].

We recently modified  $\text{Fe}_3\text{O}_4$  and  $\text{Fe}_3\text{O}_4@\text{Cu}_{2-x}\text{S}$  to produce transparent films for solar harvesting and photothermal energy generation [23–27]. The transmission electron microscopy (TEM) images of  $\text{Fe}_3\text{O}_4$  (Figure 4a) and  $\text{Fe}_3\text{O}_4@\text{Cu}_{2-x}\text{S}$  (Figure 4b) nanopar-

ticles are shown in Figure 4. As shown in this figure, the average sizes of  $\text{Fe}_3\text{O}_4$  and  $\text{Fe}_3\text{O}_4@\text{Cu}_{2-x}\text{S}$  nanoparticles are approximately 10 nm and 15 nm, respectively. The  $\text{Fe}_3\text{O}_4@\text{Cu}_{2-x}\text{S}$  solution has an absorption peak at 1160 nm due to its core-shell structure, whereas  $\text{Fe}_3\text{O}_4$  exhibits no IR absorption. The absorption of  $\text{Fe}_3\text{O}_4@\text{Cu}_{2-x}\text{S}$  nanoparticles is characterized by a “U”-shaped curve with significant absorption near UV and a broad peak at 1160 nm, as shown in Figure 4c. The IR absorption peak in  $\text{Fe}_3\text{O}_4@\text{Cu}_{2-x}\text{S}$  has been attributed to the LSPR coupling between the nanoparticles [61].

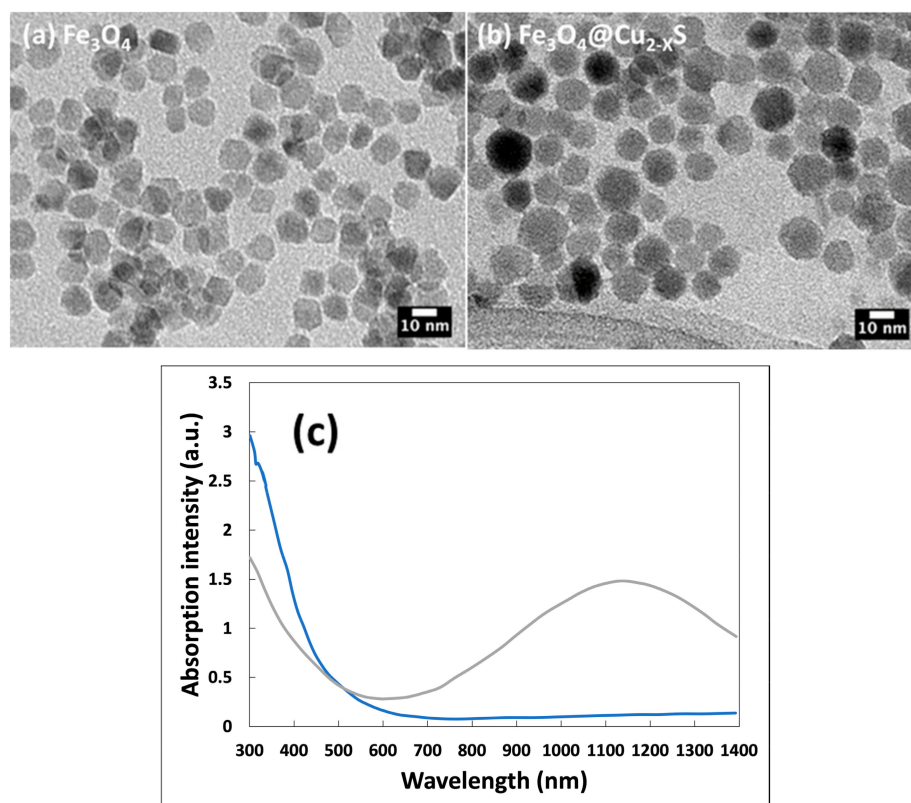


**Figure 4.** TEM micrographs of (a)  $\text{Fe}_3\text{O}_4$  and (b)  $\text{Fe}_3\text{O}_4@\text{Cu}_{2-x}\text{S}$  nanoparticles, and (c) absorptions of the  $\text{Fe}_3\text{O}_4$  (blue line) and  $\text{Fe}_3\text{O}_4@\text{Cu}_{2-x}\text{S}$  (grey line) nanoparticles [27].

#### 4. Photothermal Thin Films for 3D Solar Light Harvesting and Energy Generation

We chose  $\text{Fe}_3\text{O}_4@\text{Cu}_{2-x}\text{S}$  and chlorophyllin, among various iron oxides and porphyrins, as the base materials for depositing PT thin films due to their unique “U”<sup>27</sup> and “saddle” [19–23]-shaped absorption patterns. The  $\text{Fe}_3\text{O}_4@\text{Cu}_{2-x}\text{S}$  and chlorophyllin photothermal materials were synthesized and deposited on transparent quartz substrates [24–30,62]. To uniformly apply the solutions containing  $\text{Fe}_3\text{O}_4@\text{Cu}_{2-x}\text{S}$  or chlorophyllin, the glass substrates were spin-coated with 120  $\mu\text{L}$  of the solutions at 1000 rpm for 30 s using a WS-400-6NPP-Lite spin coater. The glass slides were first cut into  $25 \times 25 \text{ mm}^2$  substrates and cleaned by sonicating in methanol for 15 min, followed by sonicating in isopropyl alcohol for another 15 min. The thickness and concentration of the coatings on the glass substrates were varied to control the average visible transmittance (AVT), which is a critical factor in multilayer solar harvesting and was maintained in the range of 85%. AVT values were measured using a LS116 Light Transmittance Meter manufactured by Linshang Technology.

We have designed and built a solar-powered photothermal energy generator to show the feasibility of multilayer 3D solar harvesting and the conversion of simulated solar light into thermal energy in a cuboid structure comprised of multiple layers of PT films (Figure 5) [62]. As shown in Figure 5, the cuboid is made up of 10 layers of transparent PT films of either  $\text{Fe}_3\text{O}_4@\text{Cu}_{2-x}\text{S}$  or chlorophyllin, each deposited on a  $25.4 \times 25.4 \times 1.4 \text{ mm}^3$  quartz substrate. These PT-coated transparent substrates are arranged parallel to each other

within a  $5 \times 5 \times 15 \text{ cm}^3$  cuboid structure with six glass walls. When the simulated solar light source ( $0.4 \text{ W/cm}^2$ ) is turned on, the light enters the top of the cuboid and passes through each PT film substrate layer until it reaches the bottom [62].

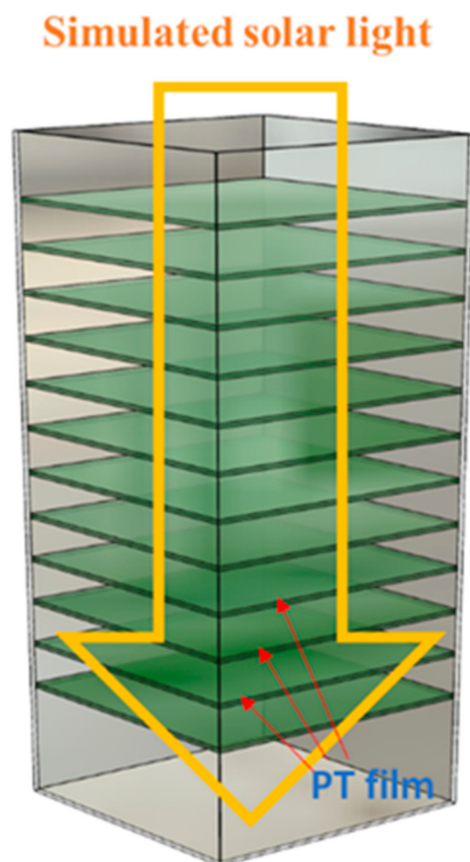


**Figure 5.** The multilayer 3D solar harvesting photothermal energy generator [62]. Reprinted with permission from Lyu, Mengyao, Jou Lin, John Krupczak, and Donglu Shi. “Solar harvesting through multilayer spectral selective iron oxide and porphyrin transparent thin films for photothermal energy generation.” *Advanced Sustainable Systems* 5, no. 6 (2021): 2100006. Copyright 2023 John Wiley and Sons.

The heating and cooling cycles are depicted in Figure 6 for films coated on quartz substrates with an AVT of 85%. Ten layers of these films are arranged in parallel in the 3D solar harvesting photothermal energy generator (Figure 5). As shown in the figure, both  $\text{Fe}_3\text{O}_4@\text{Cu}_{2-x}\text{S}$  and chlorophyllin thin films exhibit a plateau in their heating curves. The highest temperatures reached are  $76.1^\circ\text{C}$  for  $\text{Fe}_3\text{O}_4@\text{Cu}_{2-x}\text{S}$  (Figure 6a) and  $71.6^\circ\text{C}$  for chlorophyllin (Figure 6b) after 80 min of exposure to the light source. To reach even higher temperatures in the 3D solar harvesting photothermal energy generator, the heating time can be extended.

As thermal energy generation is cumulative, the maximum temperature of a 3D solar harvesting photothermal energy generator can reach a significant level based on factors such as light power intensity, thermal insulation, and duration. Figure 7 shows the infrared images of the temperature distributions of the PTG before and after light exposure for various time intervals. With the light off, the cuboid remains close to room temperature ( $25.1^\circ\text{C}$ ). Upon turning the light on for 15 min, the top part of the cuboid is heated first as the light penetrates more efficiently from the top. The lower part becomes hotter after 30 min. By 45 min, the temperature distribution is even, indicating the cumulative photothermal effect. The temperature can continue to increase for prolonged exposure to the light.

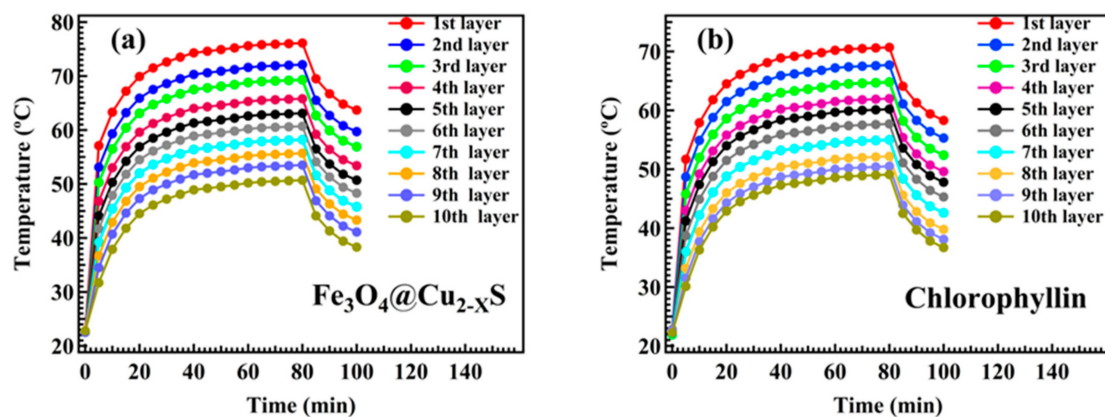


**Figure 6.** (a) Heating curves  $\text{Fe}_3\text{O}_4@\text{Cu}_{2-x}\text{S}$ , (b) heating curves of chlorophyllin in 3D solar harvesting photothermal energy generator (Figure 5) [62]. Reprinted with permission from Lyu, Mengyao, Jou Lin, John Krupczak, and Donglu Shi. “Solar harvesting through multilayer spectral selective iron oxide and porphyrin transparent thin films for photothermal energy generation.” *Advanced Sustainable Systems* 5, no. 6 (2021): 2100006. Copyright 2023 John Wiley and Sons.

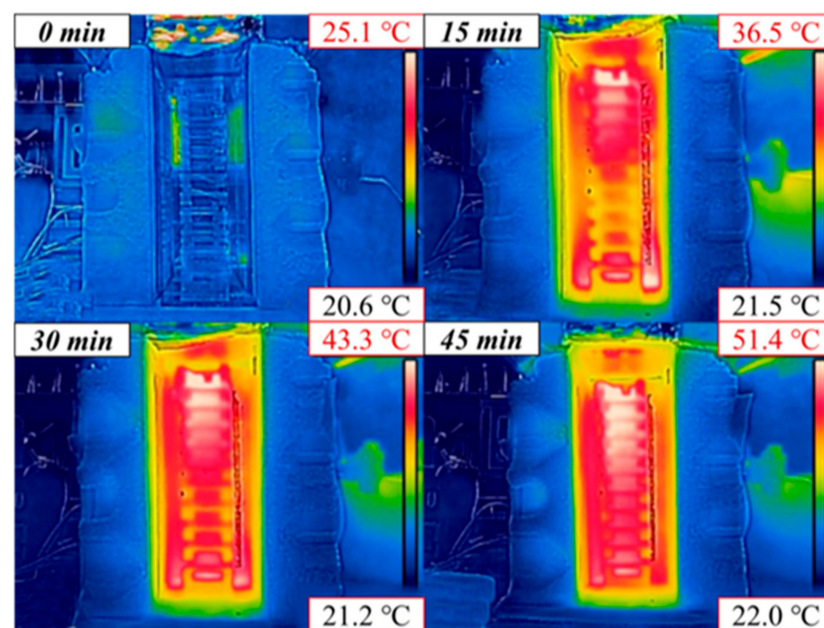


**Figure 7.** Infrared images of the 3D solar photothermal energy generator with the  $\text{Fe}_3\text{O}_4@\text{Cu}_{2-x}\text{S}$  films (85% AVT) at different time intervals. Note that the temperature can continue to rise if the light source is kept on for extended times [62]. Reprinted with permission from Lyu, Mengyao, Jou Lin, John Krupczak, and Donglu Shi. “Solar harvesting through multilayer spectral selective iron oxide and porphyrin transparent thin films for photothermal energy generation.” *Advanced Sustainable Systems* 5, no. 6 (2021): 2100006. Copyright 2023 John Wiley and Sons.

The results shown in Figures 6 and 7 provide strong experimental evidence of the ability to convert solar light into thermal energy through multilayered thin films. The thermal energy generated has a linear relationship with the number of layers, as demonstrated in Figure 8a, for both  $\text{Fe}_3\text{O}_4@\text{Cu}_{2-x}\text{S}$  and chlorophyllin systems. The thermal energy produced increased dramatically from 5074.3 J (for one layer) to 55,465.8 J (for ten layers) in the  $\text{Fe}_3\text{O}_4@\text{Cu}_{2-x}\text{S}$  system, and from 3826.3 J (for one layer) to 56,143.9 J (for ten layers) in the chlorophyllin system, both displaying over ten-fold increase. Figure 8b illustrates the linear relationship between temperature and number of layers for both  $\text{Fe}_3\text{O}_4@\text{Cu}_{2-x}\text{S}$  and chlorophyllin thin films, with maximum temperatures of 76.1 °C and 70.7 °C, respec-



tively. These temperatures have the potential to exceed 100 °C if the system parameters are optimized. The energy density inside the cuboid increases as the number of layers increases from 1 to 10, as demonstrated in Figure 8c. Specifically, for  $\text{Fe}_3\text{O}_4@\text{Cu}_{2-x}\text{S}$ , the energy density increases from  $1.35 \times 10^7 \text{ J/m}^3$  to  $1.48 \times 10^8 \text{ J/m}^3$ , and, for chlorophyllin, it increases from  $1.02 \times 10^7 \text{ J/m}^3$  to  $1.49 \times 10^8 \text{ J/m}^3$ . The film AVT, thermal insulation, and photothermal coefficients can be further enhanced to increase energy density for a harvesting photothermal energy generator.

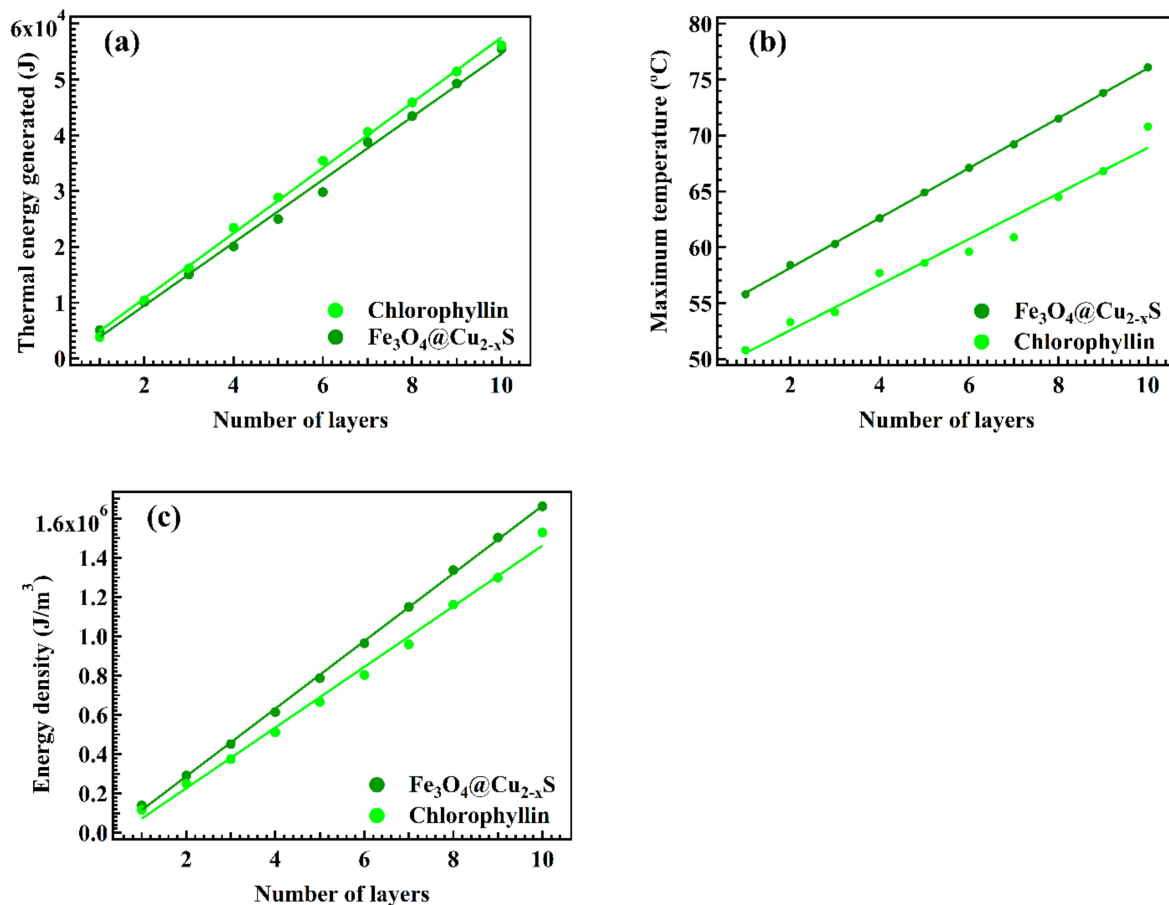


**Figure 8.** (a) Thermal energy vs. number of layers, (b) maximum temperature vs. number of layers, (c) energy density vs. number of layers for the  $\text{Fe}_3\text{O}_4@\text{Cu}_{2-x}\text{S}$  and chlorophyllin thin films for 80 min heating time in the 3D solar photothermal energy generator (Figure 5) [62]. Reprinted with permission from Lyu, Mengyao, Jou Lin, John Krupczak, and Donglu Shi. “Solar harvesting through multilayer spectral selective iron oxide and porphyrin transparent thin films for photothermal energy generation.” *Advanced Sustainable Systems* 5, no. 6 (2021): 2100006. Copyright 2023 John Wiley and Sons.

Our investigation aimed to assess the photothermal energy conversion efficiency of the 3D solar photothermal energy generator, with a focus on the viability of multilayer solar harvesting. The goal was to generate significant amounts of thermal energy using an array of PT films, thus providing stronger evidence for the feasibility of 3D solar harvesting. Based on the results shown in Figures 6–8, the solar photothermal conversion efficiency ( $\eta$ ) of  $\text{Fe}_3\text{O}_4@\text{Cu}_{2-x}\text{S}$  and chlorophyllin thin films was calculated [62]. The solar photothermal conversion efficiency represents the ratio of the energy increase within the 3D solar photothermal energy generator to the simulated solar radiation. The calculations were based on previously published methods [21,22,62]. As shown in Ref. [62],  $\eta$  increased from 40.9 (one layer) to 63.4 (ten layers) for the  $\text{Fe}_3\text{O}_4@\text{Cu}_{2-x}\text{S}$  film and from 30.9 (one layer) to 61.6 (ten layers) for the chlorophyll film, indicating a twelve-fold increase in photothermal



conversion efficiency due to the utilization of multiple layers in the 3D solar setup. These findings suggest that further improvements in solar photothermal conversion efficiency can be achieved by adding more layers.

### 5. Transparent DSSC Thin Films for 3D Solar Light Harvesting and Energy Generation

In the realm of solar energy conversion, photovoltaics is a well-known method for converting sunlight into electricity and promoting energy sustainability. Despite its widespread use, the power conversion efficiency (PCE) of photovoltaics can vary greatly depending on the materials used, from silicon to polymers [63]. The most common type of polymer solar cells (PSCs) use P3HT and PCBM polymers and have a PCE of around 13% [64–67]. Although this is significantly lower than the 20% efficiency of commercial solar panels, PSCs have the advantages of being lightweight, affordable, and flexible for various applications, such as biomedicine, remote sensors, wireless devices, and enhancing the aesthetic appeal of architectural designs and building materials.

The power conversion efficiency (PCE) of photovoltaics (PVs) can be limited, especially in non-silicon-based materials, such as polymer solar cells (PSCs), with PCE around 13 percent [63]. To enhance PCE, we designed a multilayer system, as shown in Figure 9, which is based on the concept depicted in Figures 1 and 5. This design increases the surface area exposed to sunlight and compensates for the low efficiency of the non-silicon-based materials. By considering the PCE of a 3D multilayer solar harvesting system rather than a 2D PV panel, the overall performance can be improved.

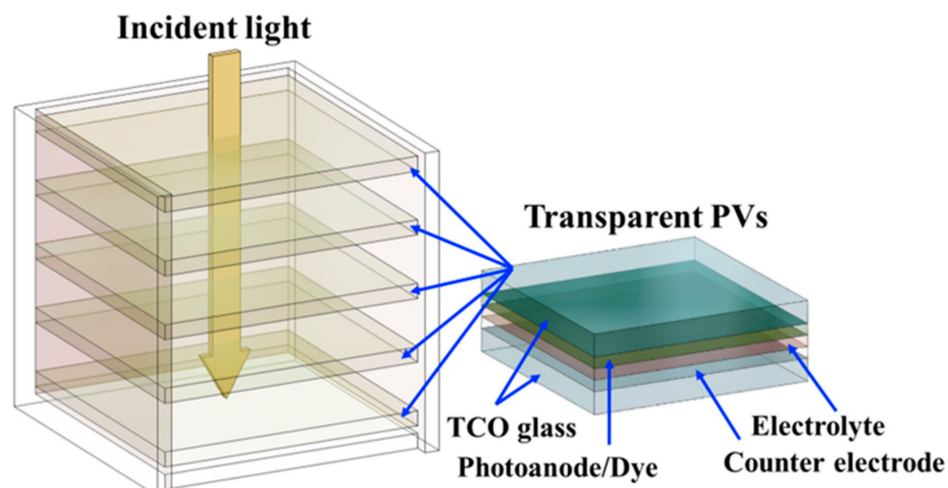


**Figure 9.** Schematic of 3D solar harvesting photovoltaic system with transparent PV films.

The primary focus of our research was to develop the transparent dye-sensitized solar cells (DSSCs) for the solar system as shown in Figure 9. DSSCs are a type of thin-film solar cell that harnesses organic dyes to capture sunlight and produce an electrical current [51,68–72]. The structure of a DSSC typically consists of a transparent conducting electrode (such as indium tin oxide or fluorine-doped tin oxide), a photosensitive dye that absorbs light, an electrolyte to transport charges from the dye to the electrode, and a counter electrode (Figure 9) [51]. In a DSSC, light is absorbed by the dye, which injects electrons into a semiconducting material, such as titanium dioxide, that forms the electrode. The electrons then travel through the electrode and electrolyte to the counter electrode, where they are collected and used to generate an electrical current [51,68–72]. DSSCs have several advantages over other types of solar cells, including low cost, flexibility, and ease of fabrication. Furthermore, the use of dyes in DSSCs provides a wider absorption spectrum compared to silicon-based solar cells, resulting in higher efficiency [51,68–72]. Despite these benefits, there are some challenges associated with DSSCs, such as the limited stability of the dyes, the requirement for an expensive transparent conducting electrode, and the limited power conversion efficiency compared to other types of solar cells.

Recently, there has been a surge in the use of porphyrins as light-harvesting materials in photovoltaic cells due to their low cost and easy synthesis, as well as their superior absorption properties [73–80]. Researchers aim to increase efficiency and lower the cost of solar energy conversion by incorporating porphyrins into photovoltaic devices. Various types of porphyrin compounds have been studied for their photovoltaic properties, including meso-tetrakis(4-sulfonatophenyl)porphyrin, zinc phthalocyanine, and porphyrin derivatives functionalized with electron-accepting or electron-donating groups [73–80]. Although the photovoltaic effect of porphyrins is promising, there is much room for improvement in terms of optimizing their performance in photovoltaic cells and enhancing their stability when exposed to light for prolonged periods. Nonetheless, the study of porphyrins as light-harvesting materials holds the potential to lead to the development of innovative and efficient photovoltaic technologies. The transparent DSSC films with porphyrins such as chlorophyllin developed in our research can also be applied to the 3D solar harvesting photovoltaic system (Figure 9). In this study, we chose N719 as the organic dye in developing the transparent DSSCs.

N719 is a well-known organic dye utilized in the photovoltaic industry, particularly in the development of dye-sensitized solar cells (DSSCs) [81–86]. N719 is an efficient light capturing dye with a broad absorption spectrum, making it ideal for use in solar energy conversion. Originally developed by Grätzel and his team [51], N719 quickly gained popularity among DSSC developers due to its exceptional stability, low cost, and impressive performance [81–86]. The dye consists of a porphyrin molecule that has been modified with electron-accepting groups, enabling it to absorb light and transfer electrons to the semiconducting electrode. Beyond its use in DSSCs, N719 has also been explored for applications in other photovoltaic devices, including perovskite solar cells and organic photovoltaics [82]. Despite a few challenges, such as limited solubility, N719 remains a favored option in the photovoltaic field due to its high efficiency and remarkable performance.

In this study, a 0.3 mM N719 solution was developed using a mixture of acetonitrile and tert-butanol in a 1:1 ratio by volume. The TiO<sub>2</sub> layer was deposited on FTO glass using the doctor blading method and was ultrasonic cleaned followed by acetone and isopropyl alcohol wash for 15 min. The TiO<sub>2</sub> layer was then dried for 30 min at 60 °C and sintered for 30 min at 500 °C. The photoelectrode was then soaked in the N719 dye solution for 20 h. The counter electrode, made of Pt, was produced by spin coating an H<sub>2</sub>PtCl<sub>6</sub> solution with 1 wt.% isopropyl onto FTO glass, followed by a 30 min sintering process at 450 °C. The solution was applied to FTO glass substrates by spin coating for 30 s at 4000 rpm using 10 µL of solution on each glass slide. Finally, a DSSC device was constructed by joining the photoanode, consisting of a TiO<sub>2</sub> layer on FTO glass, and the cathode, made of Pt on FTO glass.

The final step involved filling the photoanode and cathode with an electrolyte solution. The absorption spectra of a N719 solution with a concentration of 0.01 mg/mL in ethanol is shown in Figure 10a, highlighting peaks at 311 nm, 384 nm, and 528 nm. The band gap energy was determined from the first visible peak. As shown in the Tauc plots (Figure 10b), the direct band gap energy for N719 was calculated to be 2.12 eV. It is important to mention that the band gap energy for the anatase phase of TiO<sub>2</sub> is approximately 3.2 eV, while that of the rutile phase of TiO<sub>2</sub> is around 3 eV.

A ruthenium complex (N719) was used to develop the 3D solar harvesting photovoltaic system with transparent DSSCs films. Figure 11 illustrates the 3D solar harvesting system, which is composed of five parallel N719-DSSC thin films with a 3 cm distance between each photovoltaic layer. The simulated solar light (100 mW/cm<sup>2</sup>) is directed from the top down, illuminating the first photovoltaic and then shining through it to reach the second one underneath it. Due to the transparency of these PVs, the incident light can penetrate multiple transparent DSSCs, with the first N719-DSSC producing a peak power output of 4.88 mW, the second 0.643 mW, the third 0.269 mW, the fourth 0.136 mW, and the fifth 0.082 mW. Although the power output decreases due to reduced incoming light power, each can yield finite power, indicating the viability of the multilayered system, capable

of solar harvesting and energy generation in a 3D fashion. The power attenuation can be reduced by improving the AVT of the DSSC films.

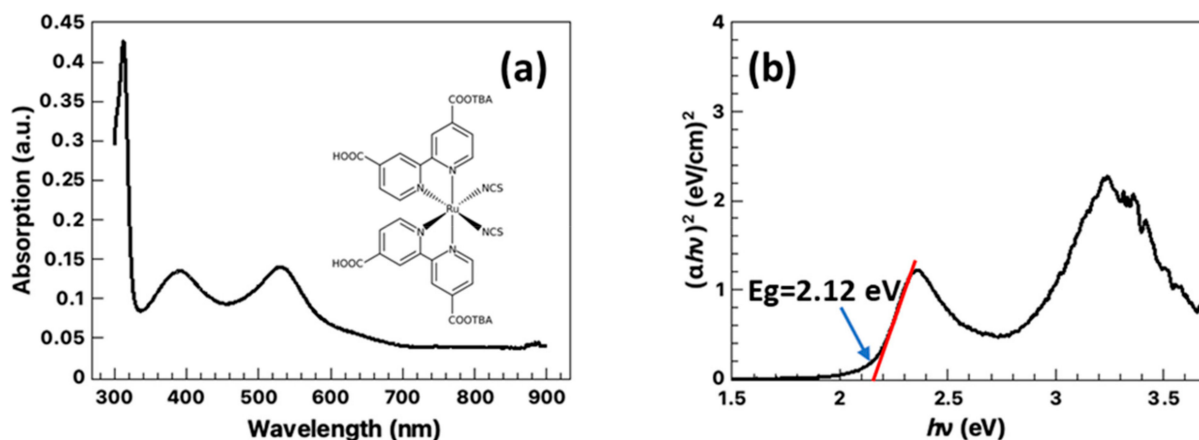


Figure 10. (a) UV-vis absorption spectra of solutions of N719 dye with molecule structure. (b) Extrapolation of the Tauc plot for bandgap calculations of N719 dye.

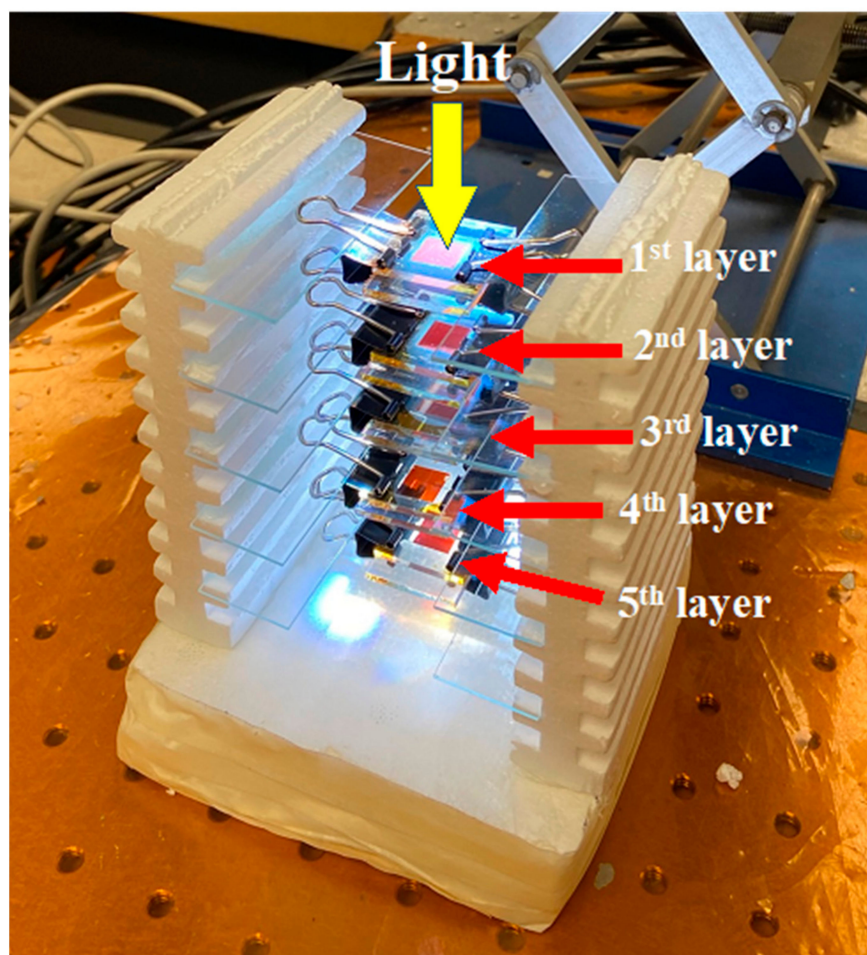


Figure 11. Photograph of 3D solar harvesting through 5 PVs.

The I–V curves for the five photovoltaics are displayed in Figure 12 for light irradiation of  $100 \text{ mW/cm}^2$ . As shown in the figure, the first layer PV exhibits a considerable maximum voltage ( $V_{\text{max}}$ ) and current ( $I_{\text{max}}$ ). However, there is a noticeable decrease in the maximum power ( $I_{\text{max}} \times V_{\text{max}}$ ) for the PVs under the first layer due to the reduced light power density.

This is a major issue that needs to be addressed in future research. Table 1 summarizes all the performance parameters of PVs at different layers. To enhance the performance, the transparency of the top PV and the distance between the PVs must be optimized. The research plan is to optimize the PV parameters, including AVT, light intensity, light incident angles, and interspacing of PVs, in order to maximize solar light harvesting through multiple layers.

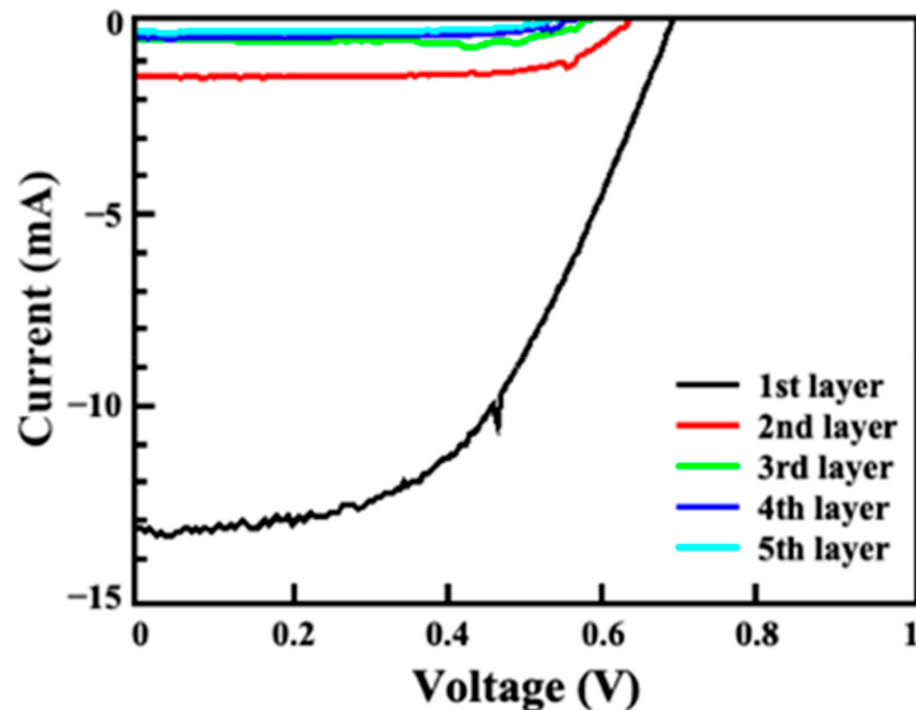


Figure 12. I–V curves of different layers of N719-DSSCs.

Table 1. The performance parameters of the N719 DSSCs under 100 mW/cm<sup>2</sup> light irradiation.

	Voc (V)	Isc (mA)	P Max (mW)	E.F.	Light Density (W/cm <sup>2</sup> )	Efficiency (%)
1st layer	0.689	13.245	4.880	0.535	0.100	4.880
2nd layer	0.629	1.406	0.643	0.727	0.017	0.643
3rd layer	0.574	0.428	0.269	1.098	0.012	0.269
4th layer	0.550	0.396	0.136	0.625	0.010	0.136
5th layer	0.519	0.241	0.082	0.658	0.006	0.082

## 6. Solar Desalination via Multilayer Transparent Photothermal Films

In pursuit of the net-zero mission declared at COP26 for 2050, researchers have conducted fundamental studies on developing an advanced desalination system that is energy-neutral, emission-free, and climate-positive. As climate change increasingly threatens freshwater supplies in vulnerable regions across the globe, it is crucial to expand the water portfolio available for potable, industrial, and agricultural uses. Desalination of abundant seawater and brackish water presents a promising solution, particularly in arid regions. Significant progress has been made in developing seawater desalination technologies to meet water demands, particularly in arid regions of the world. Currently, two primary processes in seawater desalination are multi-stage flash (MSF) and reverse osmosis [87–92]. MSF is a distillation process that vaporizes a portion of seawater into steam using countercurrent heat exchangers in multiple stages. Solar-powered membrane distillation (SPMD) for desalination is gaining worldwide popularity due to its energy-efficient characteristics [93–96]. Despite their ability to produce a substantial amount of fresh water, the high cost of these



desalination technologies makes them unsustainable and unaffordable for many regions of the world, particularly developing countries. For instance, the best desalination technology available in California today costs USD 1100 per acre foot of freshwater [97].

Another possible method of desalination is through solar water distillation [98–100]. Solar stills are typically used in remote areas with limited access to freshwater. Solar distillation uses heat to remove impurities, including salts, from water, making it relatively safe to drink. Instead of using machines and electrical power to generate heat and pressure, sunlight is harnessed to retain enough heat to create clean water vapor in the solar still. Most stills need to be around six square meters in size to produce enough water for one person per day. While current desalination technologies such as reverse osmosis (RO) effectively address rising water demands, their significant energy consumption poses a challenge to sustainable usage, particularly in areas lacking conventional power infrastructure [87–92]. Additionally, conventional desalination plants, such as RO, raise concerns about increased greenhouse emissions, air pollution, and noise.

We have developed a novel 3D photothermal solar desalination (3D-PSD) method via multilayer transparent films capable of solar harvest in a 3D fashion [101]. This concept is based on the 3D multilayer solar harvesting system as depicted in Figure 1. The thin films made of the porphyrin compounds and iron oxides are transparent, spectral-selective, and photothermally activated to raise surface temperature up to 50–80 °C under solar irradiation, resulting in rapid water evaporation on multiple layers. This novel concept is fundamentally different from the conventional solar stills with a single black layer for solar light absorption. With transparent photothermal thin films, solar light is able to pass through multiple layers, not only harvesting solar irradiation in a three-dimensional fashion but also generating heat on each layer for largely increased total surface area and energy density in comparison to the single-layer systems.

The novel approach is illustrated in Figure 13. As shown in this figure, the core component is the transparent photothermal thin film that contains various unique nanohybrids. Due to spectral-selective characteristics of the film, it preferentially absorbs UV and NIR irradiances on multilayers for photothermally converting the photon energies to thermal heat that effectively raises the film surface temperature (>80 °C). Each film is in contact with saltwater flowing on its surface. As heated, water evaporates rapidly and deposits on the condenser in the desalination process.

### Solar Still via Multilayer Transparent Photothermal Films

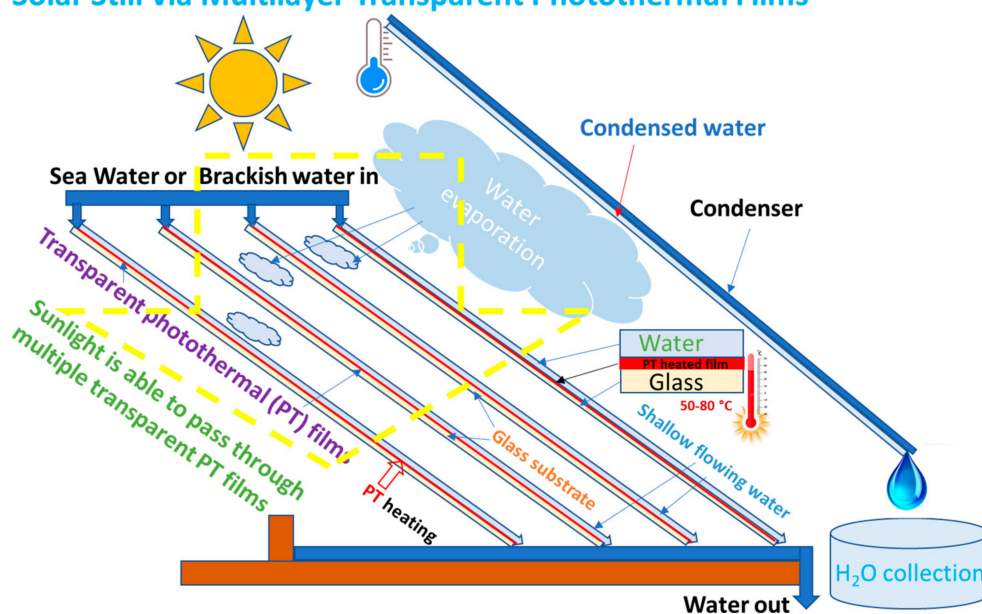


**Figure 13.** The lab-scale transparent multilayer 3D photothermal solar desalination (3D-PSD).



Based on the concepts depicted in Figure 13, we designed a 3D solar still as shown in Figure 14. Controlled by valves, seawater is flowing through the surfaces of the transparent panels in a shallow depth that are constantly heated by the photothermal coatings on the substrates, resulting in high evaporation rates. Due to multilayers, considerable volume of water can be processed at high rates depending on the total cross-sectional areas designed. The system is entirely relying on natural resources: solar light and no electrical power is required. The system can be scaled up to mega sizes in large fields, capable of producing a huge quantity of water for agricultural irrigation. While the photothermal effect is responsible for generating sufficient heat for saltwater evaporation, the light transmittance of the film allows sunlight to pass through as many layers as possible to increase the effective surface area of evaporation.

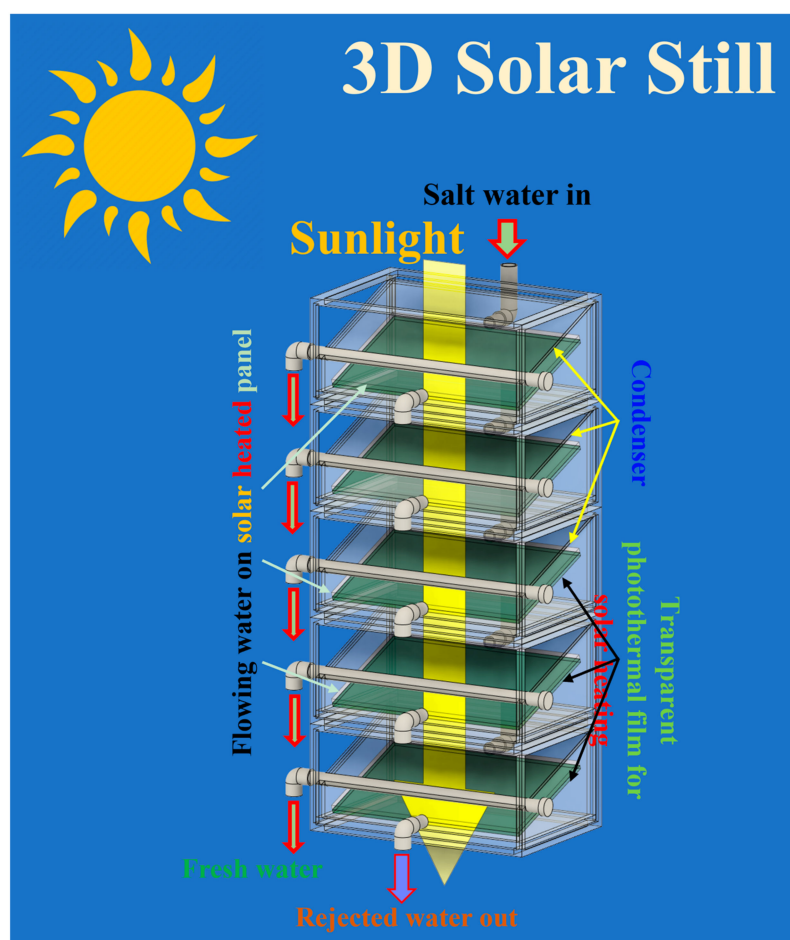


**Figure 14.** Schematic diagram showing an engineered 3D solar distillation system utilizing the transparent photothermal film in multilayers. In this system, the total solar harvesting/water surface area is significantly enlarged, therefore effectively increasing water yield in desalination.

To determine water evaporation rate, we designed a multilayer photothermal evaporation system (MPTES), as shown in Figure 15. The MPTES consisted of multiple Petri dishes (60 mm in diameter) on top of each other with 75 mm spacing between them. To create the transparent photothermal films,  $\text{Fe}_3\text{O}_4@\text{Cu}_{2-x}\text{S}$  was deposited onto glass substrates using spin coating. These substrates were attached at the bottom of the Petri dishes. The average visible transmittance (AVT) of the films was kept at 85% in all evaporation experiments by optimizing the concentration. We used a total of five dishes with  $\text{Fe}_3\text{O}_4@\text{Cu}_{2-x}\text{S}$  films attached for the water evaporation experiments in the MPTES.

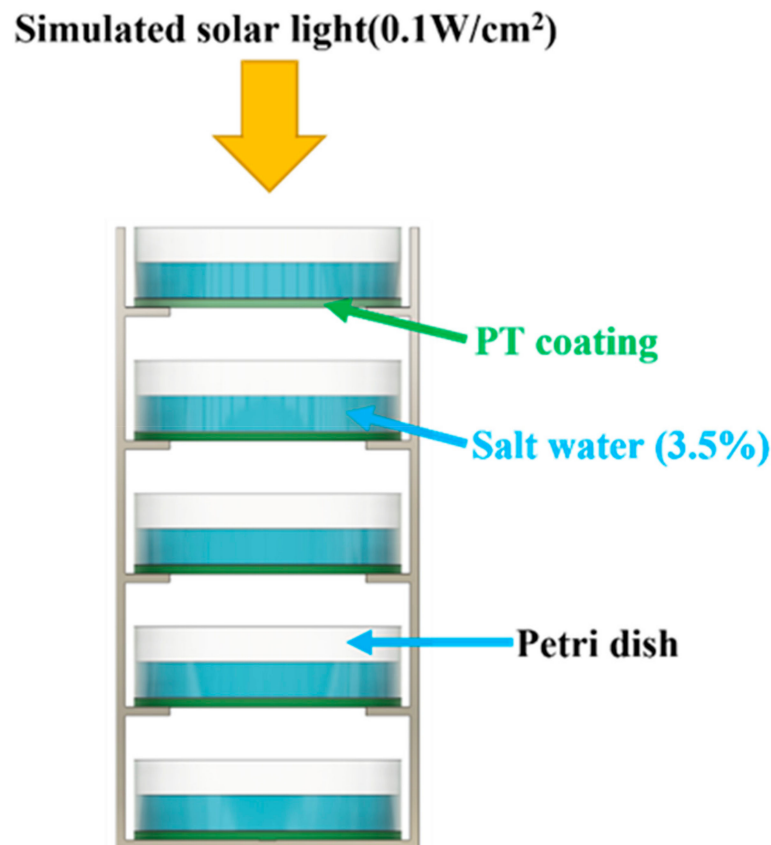


**Figure 15.** Schematic diagram showing the multilayer photothermal evaporation system (MPTES).

To investigate the effect of surface area, we determined the mass of water evaporated as a function of time for the MPTES system containing 10 mL of 3.5 wt.% saltwater without turning on the simulated solar light. It was found that the evaporation rate of the MPTES system increased 81.2% by adding four dishes to the single-dish system due to substantial increase in the total surface area (Figure 16a). While the surface area is only 28.26 cm<sup>2</sup> for a single dish, it increases to 141.3 cm<sup>2</sup> with five dishes, an increase of 400%. These results clearly indicate the effects of multilayers on the evaporation rate without any photothermal heating.

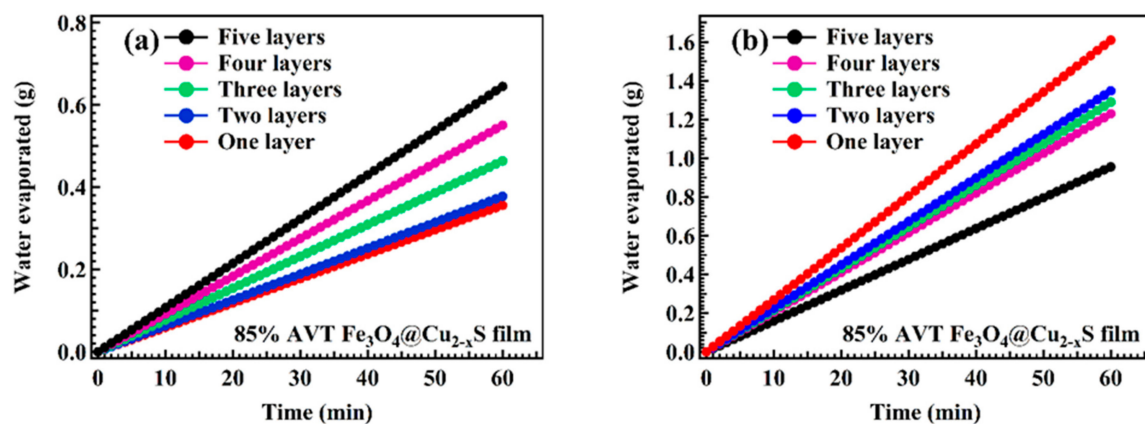


**Figure 16.** Water evaporation rate vs. time for Fe<sub>3</sub>O<sub>4</sub>@Cu<sub>2-x</sub>S-coated Petri dishes (a) without simulated solar light on and (b) with simulated solar light on.

However, turning on the simulated solar light for 60 min, the Fe<sub>3</sub>O<sub>4</sub>@Cu<sub>2-x</sub>S film was photonically activated to generate heat responsible for increased evaporation rate.

For instance, with only a single layer, the evaporation rate increased 168.3% compared with that without simulated solar light irradiation (Figure 16b). By adding four more layers, the evaporation rate increased 68.6% at 60 min and could continue to increase with prolonged light irradiation. Using the MPTES as shown in Figure 15, water evaporation can be further improved by optimizing the system parameters and the photothermal films. The photothermal effects of the thin films can be intensified for enhanced water evaporation via spectrally tuning the absorptions in UV and IR regions. By further improving AVT of the thin films, more layers can be added to the MPTES for greater water volume to be processed. A larger 3D solar distillation system can be engineered and tested with systematically controlled system parameters, including number of layers, layer spacing, layer surface area, film transparency, light powder intensity distribution over layers, and the angle of incident light. The effect of salt content on the water evaporation rate can also be investigated [22].

## 7. Issues and Challenges

The 3D system is a new approach in solar harvesting via multilayers of photothermal (PT) and photovoltaic (PV) films for improving their energy densities to utilize limited spaces. While this technology shows great promise, it also faces several challenges that need to be overcome in order to achieve its full potential. For PV cells, the 3D system will require further improvements in two major aspects, namely AVT and PCE. The former can be achieved by spectrally tuning the absorptions of PV films, while the latter may be improved by structural and material designs. As is well known, the power conversion efficiency of the PV film is limited by the intrinsic properties of the semiconducting materials as described by the SQ theory [34]. Improving PCE will require advances in both structural and material designs of PV films. For example, researchers are exploring new materials, such as perovskites [101–107], for increasing PCE via energy bandgap engineering in metal halide perovskites [108,109].

The challenges in achieving high AVT will have to be addressed for both PV and PT films for the purpose of increasing the number of layers in a 3D system leading to enhanced energy density. To increase AVT, as shown in Figure 2, the visible absorption must be further reduced via spectral tuning of the PT films, with pronounced absorptions in the UV and IR regions. One of our recent studies has achieved this goal by synthesizing a hybrid composed of the porphyrin and iron oxide compounds, specifically chlorophyllin and  $\text{Fe}_3\text{O}_4@\text{Cu}_{2-x}\text{S}$  [29]. While both pure compounds exhibit strong UV peaks, the hybrid between  $\text{Fe}_3\text{O}_4@\text{Cu}_{2-x}\text{S}$  and chlorophyllin is characterized by even stronger IR absorption. The hybrid typically exhibits a “U”-shaped absorption spectrum that simulates the ideal curve in Figure 2. Spectral tuning involves adjusting the ratio of the two compounds to match the ideal spectrum, which can significantly enhance both AVT and photothermal effect. However, achieving this ideal absorption requires novel designs of hybrids with compositional optimization.

The AVT issue is, however, more complicated in PV panels. For a silicon-based PV cell, the absorption must accommodate several conditions: (1) those photons with energies lower than the bandgap do not contribute to producing electron–hole pairs; (2) high-energy photons near UV can cause thermalization, which reduces PCE; (3) the spectral response increases with wavelength and approaches the maximum value near the bandgap. However, any absorption in the visible band will render the film less transparent. The perovskite solar cells are designed with larger bandgap energies to improve transparency [101]. Much thinner perovskite films are also produced in the order of 150–300 nm with improved transparency [101].

Overall, improving the AVT and PCE of the 3D system will require ongoing research and development efforts. However, if these challenges can be successfully addressed, the 3D system has the potential to revolutionize the field of solar energy by paving a new way in solar light harvesting and energy generation.

## 8. Summary

The area limitations of current 2D PV cells call for new approaches in more efficient solar harvesting and increased energy density. We have shown that it is highly possible to harvest solar light through multiple layers of transparent photovoltaic (PV) and photothermal (PT) thin films, therefore increasing the energy density and making more efficient use of space compared to traditional single-layer solar panels. The multilayer systems employ transparent thin films that allow solar light to pass through them for either PV or PT photon conversion and energy generation. We have investigated the optical absorption characteristics of both PT and PV, which are differently required based on their energy conversion mechanisms. The 3D solar harvesting system can provide increased energy density and space utilization as compared to traditional single-layer systems, making it a promising solution for densely populated cities with limited roof space for solar harvesting.

This review summarizes the status in the recent development of transparent porphyrin and iron oxide thin films for energy harvesting and conversion via multiple layers. The multilayer concept will profoundly transform the traditional 2D panels into a 3D solar harvesting system by increasing the sunlight collecting area in a finite volume. A 3D solar harvesting and energy generation system has been achieved based on the porphyrin and iron oxide compounds. A solar-powered photothermal energy generator (PTEG) is designed with 10 layers of  $\text{Fe}_3\text{O}_4@\text{Cu}_{2-x}\text{S}$  or chlorophyllin PT films, each deposited on quartz substrates. PTEG is illuminated by a simulated solar light source and characterized by heating and cooling cycles within a given period. The experimental results indicate that the thermal energy generated has a linear relationship with the number of layers and that the solar photothermal conversion efficiency ( $\eta$ ) increases with the number of layers, reaching maximums over 60%. The maximum temperatures reached were 76.1 °C for  $\text{Fe}_3\text{O}_4@\text{Cu}_{2-x}\text{S}$  and 71.6 °C for chlorophyllin after 80 min of exposure to the light source. These experimental results provide solid evidence on converting solar light into thermal energy through multilayered photothermal thin films.

Transparent PVs include organic photovoltaics [81–86], perovskites [101–107], and other hybrid materials [29]. However, the efficiencies of transparent photovoltaic cells are still lower compared to traditional silicon-based solar cells. This review focuses on transparent dye-sensitized solar cells (DSSCs) in a multilayered 3D solar harvesting system. DSSCs are thin-film solar cells that use organic dyes to capture sunlight and produce electrical energy. Porphyrins and N719 are well-known organic dyes used in photovoltaic devices, including DSSCs, due to their stability, low cost, and high efficiency. These materials can be deposited on different substrates as transparent DSSC films for multilayer 3D solar harvesting. Our study highlights several intriguing aspects of 3D solar harvesting and energy generation using spectral-selective materials: (1) transparent dye-sensitized solar cells with N719 show considerable power conversion efficiency; (2) the transparent solar cells can harness solar energy through multiple layers, although with limited PCE due to attenuation of incoming light power; (3) this 3D system maximizes photon utilization and generates electricity through multiple layers, opening up new avenues for sustainable solar energy technologies. The 3D system will require further improvements in two major aspects of the PV film, namely AVT and PCE. The former can be achieved by spectrally tuning the absorptions of PV films, while the latter can be improved by structural and material designs.

The advantages of the 3D solar still are several-fold: (1) no additional electric energy is needed as in the traditional desalination technologies, such as multi-stage flash and reverse osmosis processes; therefore, there are no carbon emissions, and they are particularly useful in remote arid areas; (2) the 3D multilayer channels are capable of producing desalinated water at high rates compared to those based on membranes and single-layer solar stills; and (3) the novel 3D multilayer structure can be easily scaled up for agriculture irrigation. However, the scientific challenges to be addressed are from two major aspects: (1) transparency and (2) photothermal effect of the thin films. While the photothermal effect is responsible for generating sufficient heat for saltwater evaporation, the light

transmittance of the film allows sunlight to pass through as many layers as possible to increase the effective surface area of evaporation. However, the interplay of both mechanisms requires systematic investigation. Large-scale solar desalination systems using transparent multilayer photothermal films can be developed for agriculture and drinking water in arid regions with critical water issues in the world. This novel concept will show promise to address various desalination problems, including power shortage, carbon footprint, and negative environmental impact.

**Author Contributions:** Conceptualization, D.S.; methodology, D.S., J.L. and M.L.; validation, D.S.; formal analysis, D.S., J.L. and M.L.; investigation, D.S., J.L. and M.L.; resources, D.S.; data curation, J.L. and M.L.; writing—D.S.; writing—review and editing, D.S.; visualization, D.S., J.L. and M.L.; supervision, D.S.; project administration, D.S.; funding acquisition, D.S. All authors have read and agreed to the published version of the manuscript.

**Funding:** This research was funded by National Science Foundation grant CMMI-1635089 and CMMI-1953009.

**Data Availability Statement:** Data are available in a publicly accessible repository.

**Acknowledgments:** We acknowledge the financial support from National Science Foundation CMMI-1635089 and CMMI-1953009.

**Conflicts of Interest:** The authors declare no conflict of interest.

## References

1. Parida, B.; Iniyan, S.; Goic, R. A review of solar photovoltaic technologies. *Renew. Sustain. Energy Rev.* **2011**, *15*, 1625–1636. [CrossRef]
2. Poponi, D. Analysis of diffusion paths for photovoltaic technology based on experience curves. *Sol. Energy* **2003**, *74*, 331–340. [CrossRef]
3. Mehrtash, M.; Guillermo, Q.; Yvan, D.; Daniel, R. Performance evaluation of sun tracking photovoltaic systems in Canada. In Proceedings of the 20th Annual International Conference on Mechanical Engineering-ISME 2012, Shiraz, Iran, 16–18 May 2012; pp. 16–18.
4. Mondol, J.D.; Yohanis, Y.G.; Norton, B. The impact of array inclination and orientation on the performance of a grid-connected photovoltaic system. *Renew. Energy* **2007**, *32*, 118–140. [CrossRef]
5. Fouad, M.M.; Shihata, L.A.; Morgan, E.I. An integrated review of factors influencing the performance of photovoltaic panels. *Renew. Sustain. Energy Rev.* **2017**, *80*, 1499–1511. [CrossRef]
6. Ito, M.; Kato, K.; Sugihara, H.; Kichimi, T.; Kichimi, J.; Kurokawa, K. A preliminary study on potential for very largescale photovoltaic power generation (VLSPV) system in the Gobi desert from economic and environmental viewpoints. *Sol. Energy Mater. Sol. Cells* **2003**, *75*, 507–517. [CrossRef]
7. Zhou, X.; Yang, J.; Wang, F.; Xiao, B. Economic analysis of power generation from floating solar chimney power plant. *Renew. Sustain. Energy Rev.* **2009**, *13*, 736–749. [CrossRef]
8. Cunow, E.; Giesler, B. The megawatt solar roof at the new Munich Trade Fair Centre—An advanced and successful new concept for PV plants in the megawatt range. *Sol. Energy Mater. Sol. Cells* **2001**, *67*, 459–467. [CrossRef]
9. Irace, P.; Brandon, H. Solar Heating in Commercial Buildings. Mechanical Engineering and Materials Science Independent Study. 2017. Available online: <https://openscholarship.wustl.edu/mems500/50> (accessed on 1 December 2022).
10. Available online: <https://solar.gwu.edu/how-much-land-would-it-take-power-us-solar#:~:text=According%20to%20a%202008%20analysis,1%2C948%20square%20feet%20per%20person> (accessed on 1 December 2022).
11. Building-Integrated Photovoltaics (BIPV). *Market Size, Industry Analysis Report, Regional Outlook, Application Development Potential, Price Trends, Competitive Market Share & Forecast, 2021–2027*; Allied Market Research: Portland, OR, USA, 2022.
12. Tripathy, M.; Sadhu, P.K.; Panda, S.K.; Shukla, A.K.; Sudhakar, K.; Baredar, P. A critical review on building integrated photovoltaic products and their applications. *Renew. Sustain. Energy Rev.* **2016**, *61*, 451–465. [CrossRef]
13. Taşer, A.; Koyunbaba, B.K.; Kazanasmaz, T. Thermal, daylight, and energy potential of building-integrated photovoltaic (BIPV) systems: A comprehensive review of effects and developments. *Sol. Energy* **2023**, *251*, 171–196. [CrossRef]
14. Rajoria, C.S.; Kumar, R.; Sharma, A.; Singh, D.; Suhag, S. Development of flat-plate building integrated photovoltaic/thermal (BIPV/T) system: A review. *Mater. Today* **2021**, *46*, 5342–5352. [CrossRef]
15. Ramadan, H.S.; Helmi, A.M.; Abo-Elyousr, F.K. eReview of the State-of-the-Art. *Energy Build.* **2016**, *141*, 477–488.
16. MVrcan, H.S.; Mihaljević, A.; Valić, T.; Đulbić, M. Optimal resilient facade thermal photovoltaic clustering allocation for microgrid enhanced voltage profile. *Int. J. Electr. Power Energy Syst.* **2023**, *148*, 108940. [CrossRef]
17. Lai, C.M.; Hoko, S. Solar façades: A review. *Build. Environ.* **2015**, *91*, 152–165. [CrossRef]
18. Zhang, J.; Chen, X. A Review of Material Technologies, System Design and Economics. *Energy Convers. Manag.* **2017**, *159*, 127–139.



19. Lin, J.; Shi, D. Photothermal and photovoltaic properties of transparent thin films of porphyrin compounds for energy applications. *Appl. Phys. Rev.* **2021**, *8*, 011302. [\[CrossRef\]](#)
20. Zhao, Y.; Dunn, A.; Shi, D. Effective reduction of building heat loss without insulation materials via the photothermal effect of a chlorophyll thin film coated “Green Window”. *MRS Commun.* **2019**, *9*, 675–681. [\[CrossRef\]](#)
21. Zhao, Y.; Lin, J.; Kundrat, D.M.; Bonmarin, M.; Krupczak, J.; Thomas, S.V.; Lyu, M.; Shi, D. Photonicallly-Activated Molecular Excitations for Thermal Energy Conversion in Porphyrinic Compounds. *J. Phys. Chem. C* **2020**, *124*, 1575–1584. [\[CrossRef\]](#)
22. Lyu, M.; Lin, J.; Krupczak, J.; Shi, D. Light angle dependence of photothermal properties in oxide and porphyrin thin films for energy-efficient window applications. *MRS Commun.* **2020**, *10*, 439–448. [\[CrossRef\]](#)
23. Zhao, Y.; Sadat, M.; Dunn, A.; Xu, H.; Chen, C.-H.; Nakasuga, W.; Ewing, R.C.; Shi, D. Photothermal effect on Fe<sub>3</sub>O<sub>4</sub> nanoparticles irradiated by white-light for energy-efficient window applications. *Sol. Energy Mater. Sol. Cells* **2017**, *161*, 247–254. [\[CrossRef\]](#)
24. Sadat, M.E.; Kaveh Baghbador, M.; Dunn, A.W.; Wagner, H.P.; Ewing, R.C.; Zhang, J.; Xu, H.; Pauletti, G.M.; Mast, D.B.; Shi, D. Photoluminescence and photothermal effect of Fe<sub>3</sub>O<sub>4</sub> nanoparticles for medical imaging and therapy. *Appl. Phys. Lett.* **2014**, *105*, 091903. [\[CrossRef\]](#)
25. Shi, D.; Sadat, M.E.; Dunn, A.W.; Mast, D.B. Photo-fluorescent and magnetic properties of iron oxide nanoparticles for biomedical applications. *Nanoscale* **2015**, *7*, 8209–8232. [\[CrossRef\]](#) [\[PubMed\]](#)
26. Dunn, A.W.; Ehsan, S.M.; Mast, D.; Pauletti, G.M.; Xu, H.; Zhang, J.; Ewing, R.C.; Shi, D. Photothermal effects and toxicity of Fe<sub>3</sub>O<sub>4</sub> nanoparticles via near infrared laser irradiation for cancer therapy. *Mater. Sci. Eng. C* **2015**, *46*, 97–102. [\[CrossRef\]](#)
27. Lin, J.; Zhao, Y.; Shi, D. Optical thermal insulation via the photothermal effects of Fe<sub>3</sub>O<sub>4</sub> and Fe<sub>3</sub>O<sub>4</sub>@Cu<sub>2</sub>-xS thin films for energy-efficient single-pane windows. *MRS Commun.* **2020**, *10*, 155–163. [\[CrossRef\]](#)
28. Lin, J.; Krupczak, J.; Shi, D. Solar harvesting and energy generating building skins with photothermal–photovoltaic dual-modality based on porphyrin thin films. *MRS Commun.* **2022**, *12*, 1225–1234. [\[CrossRef\]](#)
29. Lin, J.; Wang, Y.; Lyu, M.; Shi, D. Transparent porphyrin-based hybrid films for spectral selective solar harvesting and energy generation. *Sol. Energy Mater. Sol. Cells* **2022**, *243*, 15. [\[CrossRef\]](#)
30. Al-Ezzi, A.S.; Ansari, M.N.M. Photovoltaic Solar Cells. *Appl. Syst. Innov.* **2022**, *5*, 67. [\[CrossRef\]](#)
31. Sivakumar, M.B.; Sivaraj, S. A Review of Photovoltaic Cells and their Applications. *Renew. Sustain. Energy Rev.* **2018**, *94*, 67–82.
32. Murugan, S.; Shanmugam, S.; Bharathi, J.J. Advances in Photovoltaic Cells and Their Applications. *Mater. Today Proc.* **2018**, *9*, 2389–2400.
33. Lee, Y.; Ruf, T.S. Efficiency Improvements and Materials Development for Photovoltaic Cells. *Energy Technol.* **2016**, *4*, 1430–1441.
34. Li, H.L.; Wang, Y.L.; Chen, J.S.; Lu, Y.Q. Challenges and Opportunities for Photovoltaic Cells in Energy Conversion. *J. Clean. Prod.* **2017**, *165*, 49–58.
35. Shockley, W.; Queisser, H.J. Detailed Balance Limit of Efficiency of p-n Junction Solar Panels. *J. Appl. Phys.* **1961**, *32*, 510–519. [\[CrossRef\]](#)
36. Lee, Y.; Park, C.; Balaji, N.; Lee, Y.-J.; Dao, V.A. High-efficiency Silicon Solar Panels: A Review. *Isr. J. Chem.* **2015**, *55*, 1050–1063. [\[CrossRef\]](#)
37. Zhang, Y.; Jia, X.; Liu, S.; Zhang, B.; Lin, K.; Zhang, J.; Conibeer, G. A review on thermalization mechanisms and prospect absorber materials for the hot carrier solar panels. *Sol. Energy Mater. Sol. Panels* **2021**, *225*, 111073. [\[CrossRef\]](#)
38. Huang, X.; Jain, P.K.; El-Sayed, I.H.; El-Sayed, M.A. Plasmonic photothermal therapy (PPTT) using gold nanoparticles. *Lasers Med. Sci.* **2008**, *23*, 217–228. [\[CrossRef\]](#)
39. Yang, K.; Zhang, S.; Zhang, G.; Sun, X.; Lee, S.-T.; Liu, Z. Graphene in Mice: Ultrahigh In Vivo Tumor Uptake and Efficient Photothermal Therapy. *Nano Lett.* **2010**, *10*, 3318–3323. [\[CrossRef\]](#)
40. Chu, M.; Li, H.; Wu, Q.; Wo, F.; Shi, D. Pluronic-encapsulated natural chlorophyll nanocomposites for in vivo cancer imaging and photothermal/photodynamic therapies. *Biomaterials* **2014**, *35*, 8357–8373. [\[CrossRef\]](#)
41. Feng, L.; Wu, L.; Qu, X. New Horizons for Diagnostics and Therapeutic Applications of Graphene and Graphene Oxide. *Adv. Mater.* **2013**, *25*, 168–186. [\[CrossRef\]](#)
42. Yang, H.W.; Liu, H.L.; Li, M.L.; Hsi, I.W.; Fan, C.T.; Huang, C.Y.; Lu, Y.J.; Hua, M.-Y.; Chou, H.-Y.; Liaw, J.-W. Magnetic gold-nanorod/PNIPAAmMA nanoparticles for dual magnetic resonance and photoacoustic imaging and targeted photothermal therapy. *Biomaterials* **2013**, *34*, 5651–5660. [\[CrossRef\]](#)
43. Peer, D.; Karp, J.M.; Hong, S.; Farokhzad, O.C.; Margalit, R.; Langer, R. Nanocarriers as an emerging platform for cancer therapy. *Nat. Nanotechnol.* **2007**, *2*, 751–760. [\[CrossRef\]](#)
44. Layer, G.; Jahn, D.; Deery, E.; Lawrence, A.D.; Warren, M.J. Biosynthesis of Heme and Vitamin B12. *Chem. Biol.* **2010**, *7*, 445–499. [\[CrossRef\]](#)
45. Sarkar, D.; Sharma, A.; Talukder, G. Chlorophyll and chlorophyllin as modifiers of genotoxic effects. *Mutat. Res. Genet. Toxicol.* **1994**, *318*, 239–247. [\[CrossRef\]](#) [\[PubMed\]](#)
46. Gouterman, M. Spectra of porphyrins. *J. Mol. Spectrosc.* **1961**, *6*, 138–163. [\[CrossRef\]](#)
47. Cook, L.P.; Brewer, G.; Wong-Ng, W. Structural Aspects of Porphyrins for Functional Materials Applications. *Crystals* **2017**, *7*, 223. [\[CrossRef\]](#)
48. Husain, A.A.; Hasan, W.Z.W.; Shafie, S.; Hamidon, M.N.; Pandey, S.S. A review of transparent solar photovoltaic technologies. *Renew. Sustain. Energy Rev.* **2018**, *94*, 779–791. [\[CrossRef\]](#)

49. Chang, S.-Y.; Cheng, P.; Li, G.; Yang, Y. Transparent Polymer Photovoltaics for Solar Energy Harvesting and Beyond. *Joule* **2018**, *2*, 1039–1054. [CrossRef]
50. Liu, X.; Zhong, Z.; Zhu, R.; Yu, J.; Li, G. Periodic band-pass electrode enables record-performance transparent organic photovoltaics. *Joule* **2022**, *6*, 1918–1930. [CrossRef]
51. Malek, F.; Harit, T.; Cherfi, M.; Kim, B. Insights on the Synthesis of N-Heterocycles Containing Macrocycles and Their Complexion and Biological Properties. *Molecules* **2022**, *27*, 2123. [CrossRef]
52. Deng, Z.; Wu, W.; Wang, Y.; Shi, D. Progress in Circulating Tumor Cell Isolation: A Biomarkerless Approach. *eBioMedicine* **2022**, *83*, 104237. [CrossRef]
53. Chen, B.; Le, W.; Wang, Y.; Li, Z.; Wang, D.; Ren, L.; Lin, L.; Cui, S.; Hu, J.J.; Hu, Y.; et al. Targeting Negative Surface Charges of Cancer Cells by Multifunctional Nanoprobes. *Theranostics* **2016**, *6*, 1887–1898. [CrossRef]
54. Wang, F.; Pauletti, G.M.; Wang, J.; Zhang, J.; Ewing, R.C.; Wang, Y.; Shi, D. Dual surface-functionalized Janus nanocomposites of polystyrene/Fe<sub>3</sub>O<sub>4</sub>@SiO<sub>2</sub> for simultaneous tumor cell targeting and stimulus-induced drug release. *Adv. Mater.* **2013**, *25*, 3485–3489. [CrossRef]
55. Cho, H.-S.; Dong, Z.; Pauletti, G.M.; Zhang, J.; Xu, H.; Gu, H.; Wang, L.; Ewing, R.C.; Huth, C.; Wang, F.; et al. Fluorescent, Superparamagnetic Nanospheres for Drug Storage, Targeting, and Imaging: A Multifunctional Nanocarrier System for Cancer Diagnosis and Treatment. *ACS Nano* **2010**, *4*, 5398–5404. [CrossRef] [PubMed]
56. Shi, D.; Cho, H.S.; Chen, Y.; Xu, H.; Gu, H.; Lian, J.; Wang, W.; Liu, G.; Huth, C.; Wang, L.; et al. Fluorescent polystyrene-Fe<sub>3</sub>O<sub>4</sub> composite nanospheres for in vivo imaging and hyperthermia. *Adv. Mater.* **2009**, *21*, 2170–2173. [CrossRef]
57. Zhang, Z.; Liu, Y.; Wang, H.; Huang, B.; Wang, H.; Zhang, Y. Preparation and characterization of Fe<sub>3</sub>O<sub>4</sub>@Cu<sub>2</sub>-xS core-shell nanoparticles. *Mater. Sci. Eng. B* **2011**, *176*, 400–404.
58. Li, H.; Wang, X.; Zhang, X. Preparation of Fe<sub>3</sub>O<sub>4</sub>@Cu<sub>2</sub>-xS Core-Shell Nanoparticles by a Two-Step Process and Their Optical Properties. *J. Nanosci. Nanotechnol.* **2012**, *12*, 9502–9506.
59. Li, Q.; Guo, W.; Zhang, J.; Liu, L.; Song, Y.; Liu, Y. Preparation of Fe<sub>3</sub>O<sub>4</sub>@Cu<sub>2</sub>-xS Core-Shell Nanoparticles by a Simple Method and Their Magnetic Properties. *J. Nanosci. Nanotechnol.* **2013**, *13*, 574–578.
60. Zhang, Y.; Liu, Y.; Zhang, Z.; Huang, B.; Wang, Y. Preparation and Characterization of Fe<sub>3</sub>O<sub>4</sub>@Cu<sub>2</sub>-xS Core-Shell Nanoparticles with Different Shell Thicknesses. *J. Nanosci. Nanotechnol.* **2013**, *13*, 469–473.
61. Leao Andrade, A.; Domingos Fabris, J.; Zacarias Domingues, R.; Pereira, M.C. Current Status of Magnetite-Based Core@Shell Structures for Diagnosis and Therapy in Oncology Short running title: Biomedical Applications of Magnetite@Shell Structures. *Curr. Pharm. Des.* **2015**, *21*, 5417–5433. [CrossRef]
62. Tian, Q.; Hu, J.; Zhu, Y.; Zou, R.; Chen, Z.; Yang, S.; Li, R.; Su, Q.; Han, Y.; Liu, X. Sub-10 nm Fe<sub>3</sub>O<sub>4</sub>@Cu<sub>2</sub>-xS Core-Shell Nanoparticles for Dual-Modal Imaging and Photothermal Therapy. *J. Am. Chem. Soc.* **2013**, *135*, 8571–8577. [CrossRef]
63. Lyu, M.; Lin, J.; Krupczak, J.; Shi, D. Solar Harvesting through Multilayer Spectral Selective Iron Oxide and Porphyrin Transparent Thin Films for Photothermal Energy Generation. *Adv. Sustain. Syst.* **2021**, *5*, 2100006. [CrossRef]
64. Best Research-Cell Efficiencies. Available online: <https://www.nrel.gov/pv/assets/pdfs/best-research-cell-efficiencies.20190802.pdf> (accessed on 21 November 2020).
65. Wong, W.Y.; Wang, X.Z.; He, Z.; Djurišić, A.B.; Yip, C.T.; Cheung, K.Y.; Wang, H.; Mak, C.S.; Chan, W.K. Metallated conjugated polymers as a new avenue towards high-efficiency polymer solar cells. *Nat. Mater.* **2011**, *6*, 521–527. [CrossRef]
66. Chen, C.-C.; Dou, L.; Zhu, R.; Chung, C.-H.; Song, T.-B.; Zheng, Y.B.; Hawks, S.; Li, G.; Weiss, P.S.; Yang, Y. Visibly Transparent Polymer Solar Cells Produced by Solution Processing. *ACS Nano* **2012**, *6*, 7185–7190. [CrossRef] [PubMed]
67. Bates, M.; Malhado, C.; Yang, C.; Herrera, C.K.; Lunt, R.R. High Efficiency Transparent and Semi-Transparent Photovoltaics Based on a Layer-By-Layer Deposition. *Sol. RRL* **2023**, *early view*. [CrossRef]
68. Grätzel, M. Dye-Sensitized Solar Cells. *Nat. Photonics* **2009**, *3*, 145–153. [CrossRef]
69. Wu, C.; Chen, J.; Liu, Y.; Hou, J. Dye-sensitized solar cells: Recent advances and challenges. *J. Mater. Chem. A* **2016**, *4*, 7548–7564.
70. Wang, X.; Grätzel, M. Dye-sensitized solar cells: From basics to the state of the art. *Energy Environ. Sci.* **2013**, *6*, 242–269.
71. O'Regan, S.; Grätzel, M. A low-cost, high-efficiency solar cell based on dye-sensitized colloidal TiO<sub>2</sub> films. *Nature* **1991**, *353*, 737–740. [CrossRef]
72. Kim, J.; Lee, Y.; Kim, H. Dye-Sensitized Solar Cells: A Review on Materials, Devices, and Applications. *Adv. Mater.* **2010**, *22*, 1834–1850.
73. Prince, R.; Grunwaldt, J. Dye-sensitized solar cells: Materials, devices, and future perspectives. *Chem. Soc. Rev.* **2015**, *44*, 123–142.
74. Imahori, H.; Tamaki, K. Porphyrin-based solar cells. *Chem. Soc. Rev.* **2011**, *40*, 22–35.
75. Fukuzumi, S.; Saito, M.; Tanaka, T. Porphyrin-based solar cells: Recent advances and future prospects. *J. Porphyr. Phthalocyanines* **2018**, *22*, 390–408.
76. Maheshwaran, N.N.N.; Kandaswamy, K. Porphyrin-Based Solar Cells: A Review. *Sol. Energy* **2018**, *170*, 417–437.
77. Arrechea, S.; Aljarilla, A.; de la Cruz, P.; Palomares, E.; Sharma, G.D.; Langa, F. Efficiency improvement using bis(trifluoromethane) sulfonamide lithium salt as a chemical additive in porphyrin based organic solar cells. *Nanoscale* **2016**, *8*, 17953–17962. [CrossRef] [PubMed]
78. De Angelis, F.; Di Carlo, A.; Filippetti, A.; Fontanesi, C. Porphyrin-Based Dye-Sensitized Solar Cells: A First-Principles Study. *J. Phys. Chem. C* **2007**, *111*, 11558–11564.
79. Stamplecoskie, K.G.; Lim, S.S.S.; Weidman, I.M.M. Porphyrin-Based Solar Cells: Advances and Challenges. *Adv. Mater.* **2017**, *29*, 47.

80. Yella, A.; Lee, H.-W.; Tsao, H.N.; Yi, C.; Chandiran, A.K.; Nazeeruddin, M.K.; Diau, E.W.-G.; Yeh, C.-Y.; Zakeeruddin, S.M.; Grätzel, M. Porphyrin-Sensitized Solar Cells with Cobalt (II/III)-Based Redox Electrolyte Exceed 12 Percent Efficiency. *Science* **2011**, *334*, 629–634. [\[CrossRef\]](#)
81. Hupp, J.T.; Niemczyk, M.P. Porphyrins as materials platforms for molecular solar cells. *J. Mater. Chem. A* **2013**, *1*, 12773–12783.
82. Mathew, S.; Yella, A.; Gao, P.; Humphry-Baker, R.; Curchod, B.F.E.; Ashari-Astani, N.; Tavernelli, I.; Rothlisberger, U.; Nazeeruddin, K.; Graetzel, M. Dye-sensitized solar cells with 13% efficiency achieved through the molecular engineering of porphyrin sensitizers. *Nat. Chem.* **2014**, *6*, 242–247. [\[CrossRef\]](#)
83. Sharma, K.; Sharma, V.; Sharma, S.S. Dye-Sensitized Solar Cells: Fundamentals and Current Status Nanoscale. *Res. Lett.* **2018**, *13*, 381. [\[CrossRef\]](#)
84. Daeneke, T.; Kwon, T.H.; Holmes, A.B.; Duffy, N.W.; Bach, U.; Spiccia, L. High-efficiency dye-sensitized solar cells with ferrocene-based electrolytes. *Nat. Chem.* **2011**, *3*, 211–215. [\[CrossRef\]](#)
85. Ammasi, A.; Iruthayaraj, R.; Munusamy, A.P.; Shkir, M. Molecular engineering on D- $\pi$ -A organic dyes with flavone-based different acceptors for highly efficient dye-sensitized solar cells using experimental and computational study. *J. Mol. Model.* **2023**, *29*, 45. [\[CrossRef\]](#)
86. Richhariya, G.; Meikap, B.C.; Kumar, A. Review on fabrication methodologies and its impacts on performance of dye-sensitized solar cells. *Environ. Sci. Pollut. Res.* **2022**, *29*, 15233–15251. [\[CrossRef\]](#)
87. Manikandan, K.M.; Yelilarasi, A.; Pandaram, P.; Senthamaraiannan, P.; Saravanakumar, S.S.; Khan, A.; Asiri, A.M. The effect of  $\gamma$ -ray-irradiated conducting polymer electrolyte and its application of dye-sensitized solar cells to building window glass system. *J. Solid State Electrochem.* **2020**, *24*, 251–261. [\[CrossRef\]](#)
88. Banchik, L.D.; Lienhard, V.J.H. Thermodynamic analysis of a reverse osmosis desalination system using forward osmosis for energy recovery. In Proceedings of the ASME 2012 International Mechanical Engineering Congress and Exposition, Houston, TX, USA, 9–15 November 2012; Paper No. IMECE2012-86987. American Society of Mechanical Engineers: New York, NY, USA, 2012.
89. Barello, M.; Manca, D.; Patel, R.; Mujtaba, I. Operation and modeling of RO desalination process in batch mode. *Comput. Chem. Eng.* **2015**, *83*, 139–156. [\[CrossRef\]](#)
90. Efraty, A.; Barak, R.N.; Gal, Z. Closed circuit desalination—A new low energy high recovery technology without energy recovery. *Desalination Water Treat.* **2011**, *31*, 95–101. [\[CrossRef\]](#)
91. Greenlee, L.F.; Lawler, D.F.; Freeman, B.D.; Marrot, B.; Moulin, P. Reverse osmosis desalination: Water sources, technology, and today's challenges. *Water Res.* **2009**, *43*, 2317–2348. [\[CrossRef\]](#)
92. Kundzewicz, Z.W.; Mata, L.J.; Arnell, N.W.; Doll, P.; Jimenez, B.; Miller, K.; Oki, T.; Sen, Z.; Shiklomanov, I. The implications of projected climate change for freshwater resources and their management. *Hydrol. Sci. J.* **2008**, *53*, 3–10. [\[CrossRef\]](#)
93. Lienhard, V.J.H.; Mistry, K.H.; Sharqawy, M.H.; Thiel, G. *Desalination Sustainability: A Technical, Socioeconomic, and Environmental Approach*; Chapter 5 in Thermodynamics, Exergy, and Energy Efficiency in Desalination Systems; Elsevier: Amsterdam, The Netherlands, 2017.
94. Aghajani, M.; Rafiee, M.; Asghari, M. Solar desalination by membrane distillation process: A review. *Desalination* **2015**, *365*, 43–60.
95. Al-Zahrani, S.M.; Kabeel, A.E. Solar energy desalination technologies: A review. *Renew. Sustain. Energy Rev.* **2019**, *101*, 28–50.
96. Badr, H.M.; Ali, A.A. Solar-driven membrane distillation for seawater desalination: A comprehensive review. *Desalination* **2018**, *431*, 62–88.
97. Guijt, C.; Fletcher, D.F. Solar-driven membrane distillation for seawater desalination: A review. *Desalination* **2018**, *434*, 30–51.
98. California Department of Water Resources. 2018. Available online: [https://suscon.org/blog/2022/06/awm-dwr-interview/?gclid=CjwKCAjw\\_YShBhAiEiwAMomsELjzgIqgAr5BUGe97bvUc-Ade7JdXKsdKQt9Ti-qblr7QKVZPiYA0RoC3gkQAvD\\_BwE](https://suscon.org/blog/2022/06/awm-dwr-interview/?gclid=CjwKCAjw_YShBhAiEiwAMomsELjzgIqgAr5BUGe97bvUc-Ade7JdXKsdKQt9Ti-qblr7QKVZPiYA0RoC3gkQAvD_BwE) (accessed on 1 December 2022).
99. Anjaneyulu, L.; Kumar, E.A.; Sankannavar, R.; Rao, K.K. Defluoridation of drinking water and rainwater harvesting using a solar still. *Ind. Eng. Chem. Res.* **2012**, *51*, 8040–8048. [\[CrossRef\]](#)
100. O'Meagher, B.; Reid, D.; Harvey, R. *Aids to Survival: A Handbook on Outback Survival*, 25th ed.; Western Australia Police Academy: Maylands, Australia, 2017; p. 24. ISBN 0-646-36303-4.
101. Lyu, M.; Lin, J.; Shi, D. Solar Desalination via Multilayers of Transparent Photothermal Fe<sub>3</sub>O<sub>4</sub>@Cu<sub>2</sub>-xS Thin Films. *Energy Technol.* **2021**, *9*, 11. [\[CrossRef\]](#)
102. Rahmany, S.; Etgar, L. Semitransparent Perovskite Solar Cells. *ACS Energy Lett.* **2020**, *5*, 1519–1531. [\[CrossRef\]](#)
103. Chu, W.; Li, X.; Li, S.; Hou, J.; Jiang, Q.; Yang, J. High-Performance Flexible Perovskite Solar Cells with a Metal Sulfide Electron Transport Layer of SnS<sub>2</sub> by Room-Temperature Vacuum Deposition. *CS Appl. Energy Mater.* **2019**, *2*, 382–388. [\[CrossRef\]](#)
104. Keshtmand, R.; Zamani-Meymian, M.-R.; Fallah, M. Enhanced Performance of Planar Perovskite Solar Cells Using Thioacetamide-Treated SnS<sub>2</sub> Electron Transporting Layer Based on Molecular Ink. *Energy Fuels* **2022**, *36*, 5897–5909. [\[CrossRef\]](#)
105. Dkhili, M.; Lucarelli, G.; De Rossi, F.; Taheri, B.; Hammedi, K.; Ezzaouia, H.; Brunetti, F.; Brown, T.M. Attributes of High-Performance Electron Transport Layers for Perovskite Solar Cells on Flexible PET versus on Glass. *ACS Appl. Energy Mater.* **2022**, *5*, 4096–4107. [\[CrossRef\]](#)
106. Gao, Y.; Huang, K.; Long, C.; Ding, Y.; Chang, J.; Zhang, D.; Etgar, L.; Liu, M.; Zhang, J.; Yang, J. Flexible Perovskite Solar Cells: From Materials and Device Architectures to Applications. *ACS Energy Lett.* **2022**, *7*, 1412–1445. [\[CrossRef\]](#)
107. Mahapatra, A.D.; Basak, D. Biodegradable Filter Paper Based Broad-Band Photodetection by Chemical Bath Deposited SnS<sub>2</sub> 2D-Nanosheet Array Film. *ACS Appl. Electron. Mater.* **2021**, *3*, 2114–2122. [\[CrossRef\]](#)

108. Tan, Y.; Xiao, B.; Xu, P.; Luo, Y.; Jiang, Q.; Yang, J. Improving the Photovoltaic Performance of Flexible Solar Cells with Semitransparent Inorganic Perovskite Active Layers by Interface Engineering. *ACS Appl. Mater. Interfaces* **2021**, *13*, 20034–20042. [[CrossRef](#)]
109. Hu, Z.; Lin, Z.; Su, J.; Zhang, J.; Chang, J.; Hao, Y. A Review on Energy Band-Gap Engineering for Perovskite Photovoltaics. *Sol. RRL* **2019**, *13*, 1900304. [[CrossRef](#)]

**Disclaimer/Publisher’s Note:** The statements, opinions and data contained in all publications are solely those of the individual author(s) and contributor(s) and not of MDPI and/or the editor(s). MDPI and/or the editor(s) disclaim responsibility for any injury to people or property resulting from any ideas, methods, instructions or products referred to in the content.